LETTER **Communicated by Alfonso Renart**

Mechanisms That Modulate the Transfer of Spiking Correlations

Robert Rosenbaum
robertr@math.uh.edu
Department of Mathematics, University of Houston, Houston, TX 77004, U.S.A.

Krešimir Josić
josic@math.uh.edu
Departments of Mathematics and of Biology and Biochemistry, University of Houston, Houston, TX 77004, U.S.A.

Correlations between neuronal spike trains affect network dynamics and population coding. Overlapping afferent populations and correlations between presynaptic spike trains introduce correlations between the inputs to downstream cells. To understand network activity and population coding, it is therefore important to understand how these input correlations are transferred to output correlations. Recent studies have addressed this question in the limit of many inputs with infinitesimal postsynaptic response amplitudes, where the total input can be approximated by gaussian noise. In contrast, we address the problem of correlation transfer by representing input spike trains as point processes, with each input spike eliciting a finite postsynaptic response. This approach allows us to naturally model synaptic noise and recurrent coupling and to treat excitatory and inhibitory inputs separately. We derive several new results that provide intuitive insights into the fundamental mechanisms that modulate the transfer of spiking correlations.

1 Introduction

The amount of information carried by neuronal populations can be strongly modulated by correlations in neuronal activity (Zohary, Shadlen, & Newsome, 1994; Sompolinsky, Yoon, Kang, & Shamir, 2001; Averbeck, Latham, & Pouget, 2006), and the structure of correlations can encode information about a stimulus (Vaadia et al., 1995; Dan, Alonso, Usrey, & Reid, 1998; Maynard et al., 1999; Shlens et al., 2006; Biederlack et al., 2006; Temereanca, Brown, & Simons, 2008). An understanding of how correlated variability is propagated is therefore central to understanding coding in neural tissue.

Synaptic divergence introduces correlated variability between the activity of nearby cells (Shadlen & Newsome, 1998), and synaptic convergence

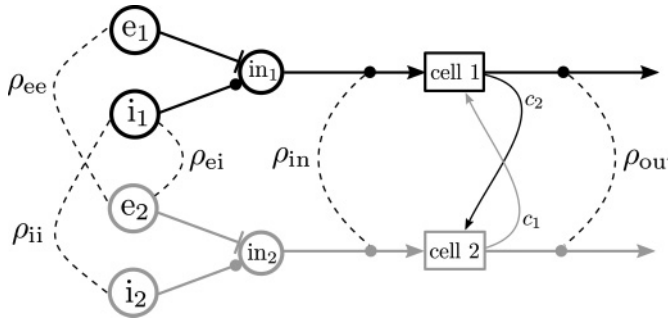

Figure 1: An abstract representation of the input-output model. Two cells each receive correlated excitatory, $e_j(t)$, and inhibitory, $i_j(t)$, inputs. These are combined to obtain the total input currents, $in_j(t)$, which drive two integrate-and-fire neurons, IF_j, to produce output spike trains, $out_j(t)$. In some of our analysis, we consider coupling between the cells. We seek to understand how the correlation, ρ_{out}, between the output spike trains is related to the statistics of the inputs and the dynamical properties of the neurons.

downstream can dramatically amplify correlations (Renart et al., 2010; Rosenbaum, Trousdale, & Josić, 2010). In the absence of mechanisms to modulate these correlations, highly correlated activity can develop in deeper layers (Reyes, 2003). However, correlations measured in vivo tend to be small (Ecker et al., 2010; Renart et al., 2010). Some recent studies show that correlations can be modulated by network effects (Hertz, 2010; Renart et al., 2010). Here, we examine how stochastic dynamics at the cellular level modulate correlations between the outputs of two cells (see Figure 1).

Earlier analytical approaches to this problem relied on the assumption that inputs can be modeled by correlated Gaussian noise (Moreno-Bote & Parga, 2006, 2010; de la Rocha, Doiron, Shea-Brown, Josić, & Reyes, 2007; Ostojić, Brunel, & Hakim, 2009; Vilela & Lindner, 2009). Such models are obtained in the limit of a large number of inputs, each of vanishing strength (Renart, Brunel, & Wang, 2003), and may not fully capture the statistical properties of the neurons' responses (Helias, Deger, Rotter, & Diesmann, 2010).

In the models we consider, inputs are represented by point processes, with each input spike having a finite impact on the membrane potential of a cell. This approach allows us to examine the effects of synaptic failure, random synaptic amplitudes, and recurrent coupling between cells while maintaining a more direct connection to physiology. Moreover, excitatory and inhibitory inputs can be treated separately (see Figure 1). We find that the effects of synaptic noise and excitatory-to-inhibitory correlations, which are often ignored when inputs are modeled as gaussian noise, can greatly reduce output correlations. Such reductions in correlation from

Table 1: Notation for Parameters and Spike Train Statistics.

$\mathrm{e}_j(t)$, $\mathrm{i}_j(t)$, $\mathrm{out}_j(t)$	Spike trains: excitatory input, inhibitory input, and output for neuron $j = 1, 2$
$\mathrm{in}_1(t)$, $\mathrm{in}_2(t)$	Total input: $\mathrm{in}_j(t) = \mathrm{e}_j(t) - \mathrm{i}_j(t)$
$N_{\mathrm{e}_j}(t)$, $N_{\mathrm{i}_j}(t)$, $N_{\mathrm{in}_j}(t)$, $N_{\mathrm{out}_j}(t)$	Spike counts: $N_X(t) = \int_0^t X(s)\,ds$
r_{e}, r_{i}, r_{out}	Firing rates: excitatory, inhibitory, and output
q	Excitation-to-inhibition balance: $q = \frac{r_{\mathrm{e}}}{r_{\mathrm{i}}}$
σ^2_{e}, σ^2_{i}, σ^2_{in}, σ^2_{out}	Asymptotic spike count variances
F_{e}, F_{i}, F_{out}	Asymptotic Fano factors: $F_x = \frac{\sigma_x^2}{r_x}$
$\mathrm{CV}_{\mathrm{out}}$	Output coefficient of variation
γ_{ee}, γ_{ii}, γ_{ei}, γ_{in}, γ_{out}	Asymptotic spike count covariances: Excitatory-to-excitatory, inhibitory-to-inhibitory, excitatory-to-inhibitory, total input, and output-to-output
ρ_{ee}, ρ_{ii}, ρ_{ei}, ρ_{in}, ρ_{out}	Asymptotic spike count correlations: $\rho_{xy} = \gamma_{xy}/(\sigma_x\sigma_y)$
S_{out}	Output synchrony, $S_{\mathrm{out}} = \frac{r_{\mathrm{synch}}}{r_{\mathrm{out}}}$, where r_{synch} is the rate of synchronous output spikes
θ, β	Threshold and lower boundary for IF models
τ_m	Membrane time constant for the LIF model
I_L	Mean leak current for the dLIF model
τ_{mem}	Memory timescale for the dLIF model

Note: We assume symmetry between cells (e.g., $r_{\mathrm{e}_1} = r_{\mathrm{e}_2} = r_{\mathrm{e}}$) throughout the text, except in the appendixes.

input to output may partly explain small correlations sometimes observed in vivo (Ecker et al., 2010; Renart et al., 2010).

To obtain a clearer understanding of how the internal dynamics of spiking neurons affect correlations, we study correlation transfer for random-walk neuronal models. These models are drastic simplifications of detailed neuron models; however, they have the advantage of being mathematically tractable while capturing essential features of the response of spiking cells (Fusi & Mattia, 1999; Salinas & Sejnowski, 2000; Rauch, La Camera, Luscher, Senn, & Fusi, 2003). Due to the simplicity of these models, our results can be understood using intuitive and mechanistic explanations. We verify that physiologically more realistic models behave similarly by comparing our analytical results with simulations.

2 Methods

We start by introducing the formalism and notation used in this work (for a concise summary of notation, see Table 1).

2.1 Spike Trains and Correlations. Spike trains are represented as stationary point processes, $a(t) = \sum_i \delta(t - t_i)$ where $\delta(t)$ denotes the Dirac function and $\{t_i\}_{i=1}^{\infty}$ is the set of spike times (Cox & Isham, 1980; Daley & Vere-Jones, 2003). The process $N_a(t) = \int_0^t a(s)\,ds$ counts the number of spikes

in the interval $[0, t]$, and $N_a(t_1, t_2) = \int_{t_1}^{t_2} a(s)\,ds$ counts the number of spikes in $[t_1, t_2]$. Stationarity implies constant firing rates $r_a = E[a(t)] = E[N_a(t)]/t$, where $E[\cdot]$ denotes expected value. The second-order statistics are quantified using the covariance and variance of spike counts,

$$\gamma_{ab}(t) = \mathrm{cov}(N_a(t), N_b(t)) \quad \text{and} \quad \sigma_a^2(t) = \gamma_{aa}(t),$$

which are related to the cross-covariance functions by

$$\gamma_{ab}(t) = \int_{-t}^{t} R_{ab}(s)(t - |s|)\,ds, \tag{2.1}$$

where $R_{ab}(\tau) = \mathrm{cov}(a(t), b(t + \tau)) = r_b(H_{ab}(\tau) - r_a)$ is the cross-covariance function, and

$$H_{ab}(\tau) = \lim_{\delta \to 0} \Pr(N_b(\tau, \tau + \delta) > 0 \,\big|\, N_a(0, \delta) > 0)/\delta$$

is the conditional firing rate (Cox & Lewis, 1972; Brody, 1999). The correlation coefficient is then given by $\rho_{ab}(t) = \gamma_{ab}(t)/(\sigma_a(t)\sigma_b(t))$. We mostly focus on the asymptotic statistics,

$$\gamma_{ab} = \lim_{t \to \infty} \gamma_{ab}(t)/t, \quad \sigma_a^2 = \gamma_{aa}, \quad \text{and} \quad \rho_{ab} = \gamma_{ab}/(\sigma_a \sigma_b),$$

which can alternately be defined using the relation $\gamma_{ab} = \int_{-\infty}^{\infty} R_{ab}(s)\,ds$.

The Fano factor, $F_a = \sigma_a^2/r_a$, is a measure of the variability, or randomness, in a spike train. For renewal spike trains, $F_a = \mathrm{CV}_a^2$ where CV_a is the coefficient of variation (CV) of the interspike interval distribution (Cox, 1962; Nawrot et al., 2008).

A measure of exact synchrony between spike trains a and b is

$$S_{ab} = r_{a \cdot b}/\sqrt{r_a r_b} = \lim_{t \to 0} \rho_{ab}(t),$$

where $r_{a \cdot b} = \lim_{\delta \to 0} \int_{-\delta}^{\delta} R_{ab}(s)\,ds$ is the rate of spikes occurring at precisely the same time. Precisely synchronous spikes can occur in integrate-and-fire models with finite, instantaneous synaptic responses whenever two neurons receive exactly synchronous excitatory input spikes. Although exactly synchronous spikes are a mathematical idealization, S_{ab} models the proportion of output spike pairs caused by a shared excitatory input in physiological settings.

2.2 The Leaky Integrate-and-Fire Model. Throughout this letter, we compare analytical results to simulations of a current-based leaky

integrate-and-fire model (the LIF). The membrane potential of the LIF is described by Tuckwell (1988) and Burkitt (2006),

$$dV = -\frac{1}{\tau_m}(V - V_{\text{rest}})\,dt + \overline{d_{\text{e}}}\,\text{e}(t)\,dt - \overline{d_{\text{i}}}\,\text{i}(t)\,dt, \tag{2.2}$$

where $\text{e}(t)$ and $\text{i}(t)$ are the excitatory and inhibitory input spike trains, respectively, and $\tau_m > 0$ is the membrane time constant (Burkitt, 2006). When $V(t)$ reaches threshold, θ, an output spike is produced, and $V(t)$ is set to V_{reset}. To simulate an inhibitory reversal potential, a lower barrier on the membrane potential is imposed at $\beta \le V_{\text{reset}}$. For simplicity, we assume that $\overline{d_{\text{e}}} = \overline{d_{\text{i}}}$. This assumption is relaxed in a later section and in the appendix by allowing variable synaptic responses. Voltage is measured in units of the postsynaptic amplitude so that $\overline{d_{\text{e}}} = \overline{d_{\text{i}}} = 1$. Due to our choice of units, the leak current when the membrane potential is at $V = v$ is given by v/τ_m. The maximum leak current is therefore θ/τ_m. We set $V_{\text{reset}} = V_{\text{rest}} = 0$, and in simulations we use $\theta = 30$ and $\beta = -2$.

The output spike train, $\text{out}(t)$, is a point process consisting of times at which the membrane potential, $V(t)$, reaches threshold. In all examples considered, $V(t)$ is an ergodic process (Stratonovich, 1963), and in all analysis, $V(0)$ is assumed to be drawn from the stationary distribution of $V(t)$ so that the output spike train is stationary.

2.3 Statistics of the Input Spike Trains. We consider two cells, $j = 1, 2$, each of which receives excitatory and inhibitory input spike trains, $\text{e}_j(t)$ and $\text{i}_j(t)$. Although more general results are derived in the appendixes, several assumptions are made in the text to keep the presentation less burdensome. In particular, we assume that the inputs to the two cells are statistically identical: $r_{\text{e}_1} = r_{\text{e}_2} = r_{\text{e}}$, $r_{\text{i}_1} = r_{\text{i}_2} = r_{\text{i}}$, $\sigma^2_{\text{e}_1} = \sigma^2_{\text{e}_2} = \sigma^2_{\text{e}}$, $\sigma^2_{\text{i}_1} = \sigma^2_{\text{i}_2} = \sigma^2_{\text{i}}$, $\gamma_{\text{e}_1\text{i}_2} = \gamma_{\text{i}_1\text{e}_2} = \gamma_{\text{ei}}$, and $\gamma_{\text{e}_1\text{i}_1} = \gamma_{\text{e}_2\text{i}_2} = 0$. The assumption that $\gamma_{\text{e}_1\text{i}_1} = \gamma_{\text{e}_2\text{i}_2} = 0$ may not hold in general (Okun & Lampl, 2008). However, correlations between the inputs to a cell simply change the input variances, σ^2_{in}, and their effect has been studied (Salinas & Sejnowski, 2000, 2002). To incorporate such correlations in our model, one substitutes $\sigma^2_{\text{in}} = \sigma^2_{\text{e}} + \sigma^2_{\text{i}} - 2\gamma_{\text{e}_j\text{i}_j}$.

We denote the excitation-to-inhibition ratio by $q = r_{\text{e}}/r_{\text{i}}$. Due to our choice of units, the excitatory and inhibitory input currents to cell j are the point processes, $\text{e}_j(t)$ and $-\text{i}_j(t)$, with mean values r_{e} and r_{i}, respectively. The total input current is given by $\text{in}_j(t) = \text{e}_j(t) - \text{i}_j(t)$ with mean $\mu_{\text{in}} = E[\text{in}_j(t)] = r_{\text{e}} - r_{\text{i}}$, variance $\sigma^2_{\text{in}} = \sigma^2_{\text{e}} + \sigma^2_{\text{i}}$, and correlation

$$\rho_{\text{in}} = \rho_{\text{in}_1\text{in}_2} = \frac{\rho_{\text{ee}}\sigma^2_{\text{e}} + \rho_{\text{ii}}\sigma^2_{\text{i}} - 2\rho_{\text{ei}}\sigma_{\text{e}}\sigma_{\text{i}}}{\sigma^2_{\text{e}} + \sigma^2_{\text{i}}}, \tag{2.3}$$

where $\rho_{ee} = \rho_{e_1e_2}$, $\rho_{ii} = \rho_{i_1i_2}$, and $\rho_{ei} = \rho_{e_1i_2} = \rho_{e_2i_1}$ are the excitatory-to-excitatory, inhibitory-to-inhibitory, and excitatory-to-inhibitory correlations (Shadlen & Newsome, 1998; Salinas & Sejnowski, 2000). To generate pairs and quadruples of correlated spike trains for simulations, we used the algorithms outlined in appendix A.

2.4 Statistics of the Output Spike Trains. In addition to symmetry between the input statistics, we also assume that the two neurons are dynamically identical (this is also relaxed in the appendixes). Hence, the output spike trains, $\text{out}_j(t)$, are statistically identical. Define the rate, variance, covariance, Fano factor, synchrony, and correlation of the two output spike trains as $r_{out} = r_{\text{out}_j}$, $\sigma^2_{out} = \sigma^2_{\text{out}_j}$, $\gamma_{out} = \gamma_{\text{out}_1\text{out}_2}$, $F_{out} = \sigma^2_{out}/r_{out}$, $S_{out} = S_{\text{out}_1\text{out}_2}$, and $\rho_{out} = \rho_{\text{out}_1\text{out}_2} = \gamma_{out}/\sigma^2_{out}$, respectively. When the outputs are renewal processes, the output coefficient of variation is given by $\text{CV}_{out} = \sqrt{F_{out}}$.

In appendix C, we use the renewal properties of the output spike trains and the Markov properties of the membrane potentials for the LIF and dLIF models with Poisson inputs to derive the following expression for the output correlation:

$$\rho_{out} = \frac{\text{CV}^2_{out} + 1}{\text{CV}^2_{out}} \left(\frac{E[\tau_1] - E[\tau_1 | V_2 \nearrow \theta]}{E[\tau_1]} \right) + \frac{S_{out}}{\text{CV}^2_{out}}. \tag{2.4}$$

Here $E[\tau_1 | V_2 \nearrow \theta]$ is the expected time until the next spike in neuron 1 given that neuron 2 has just spiked, and $E[\tau_1] = \left(\text{CV}^2 + 1\right) / (2r_{out})$ is the expected time until the next spike in neuron 1 starting from an arbitrary initial time (referred to in Cox, 1962, as the expected recurrence time). This expression is exact for uncoupled integrate-and-fire models and instantaneous synapses and white inputs. It is approximately valid for coupled models receiving nonwhite inputs or noninstantaneous synapses in the fluctuation-dominated regime. We are unaware of a similar expression in the literature, and we use it in section 4 to analyze the transfer of correlations in the fluctuation-dominated regime. The expression is also useful for calculating asymptotic correlations in simulated data. We found it to be much faster and more accurate than standard methods for calculating the correlation between two LIF neurons (see the discussion in appendix C).

2.5 The Drift-Dominated Regime and the Perfect Integrate-and-Fire Model. In drift-dominated regimes, where the excitatory current dominates the inhibitory and leak currents ($r_e \gg r_i + \theta/\tau_m$), the lower reflecting barrier at β is visited rarely. In addition, the dynamics of the neuron are dominated by the input, and a good approximation is obtained by ignoring the leak current (see Figure 2C). We therefore approximate the LIF in drift-dominated regimes by the analytically tractable perfect

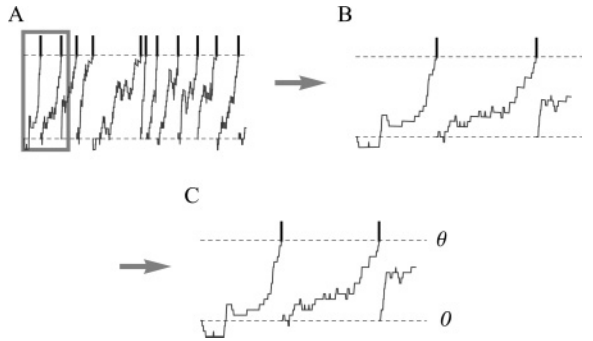

Figure 2: An LIF in the drift-dominated regime can be approximated with a PIF. (A) Typical behavior of an LIF in a drift-dominated regime ($r_e = 2.5$ KHz, $r_i = 1$ KHz, $\tau_m = 20$ ms, and $\theta = 15$). (B) Same as A, except time was rescaled using the fast-input timescale, so that B represents the region inside the gray box in A. (C) The response of a PIF driven by the same input.

integrate-and-fire (PIF) model, which is obtained by setting $1/\tau_m = 0$ in equation 2.2 and ignoring the lower boundary at β (Gerstein & Mandelbrot, 1964; Knight, 1972).

Note that the PIF model is a good approximation when the membrane time constant is slow compared to inputs and the cells integrate their inputs. It is not a good approximation when the membrane time constant is fast and the membrane potentials track their inputs, as occurs in conductance-based models in high-conductance states.

The output statistics of the PIF can be obtained analytically. When $\mu_{in} = r_e - r_i > 0$, the output rate is $r_{out} = \mu_{in}/\theta$, and when $\mu_{in} \leq 0$, the output rate is zero. Thus, the rate transfer function of the PIF is threshold linear. Hereafter, we assume that $\mu_{in} > 0$ when considering the PIF model. The total variances of the output spike trains and Fano factor are $\sigma^2_{out} = (\sigma^2_e + \sigma^2_i)/\theta^2$ and $F_{out} = (\sigma^2_e + \sigma^2_i)/[\theta(r_e - r_i)]$, respectively (see appendix B). For Poisson inputs, this yields $CV_{out} = \sqrt{(q+1)/[\theta(q-1)]}$ where $q = r_e/r_i > 1$ measures the excitation-to-inhibition balance. In Figure 3, the output rate and CV are plotted as dashed lines.

2.6 Discrete LIF Model. Outside the drift-dominated regime, spiking is increasingly due to fluctuations of the membrane potential around its mean value (Salinas & Sejnowski, 2000; Ringach & Malone, 2007). In such regimes, the PIF no longer provides a good approximation, and we instead use the analytically tractable discrete LIF (dLIF) model, which is defined by

$$dV = e(t)\,dt - i(t)\,dt - I_L(t)\,dt, \tag{2.5}$$

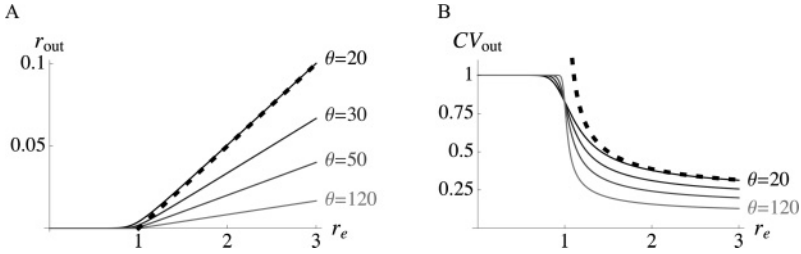

Figure 3: Univariate spiking statistics for the dLIF. (A) The output firing rate and (B) the output CV as functions of the excitatory input rate, r_e, for $\beta = -2$ and for $\theta = 20, 30, 50$, and 120. The dashed lines show the output statistics of the PIF when $\theta = 20$ and $r_i = 1$. Both r_e and r_{out} are in units of $r_i + \bar{I}_L$ (equivalently, $r_i + \bar{I}_L = 1$ is fixed) so that $\hat{q} = r_e$.

with a threshold at θ, reset at 0, and a reflecting lower boundary at $\beta \leq 0$. Here, $I_L(t) = \sum_i \delta(t - t_i)$ is a Poisson point process with rate $\bar{I}_L$ that models a leak current. Using Poisson jumps to model leak may at first seem unnatural. However, the dLIF can be thought of as a noisy integrate-and-fire model with constant leak (Fusi & Mattia, 1999). We use the dLIF because it is analytically tractable and captures the fundamental properties of correlation transfer in more realistic leaky models.

In parameter regimes where the input currents dominate the leak current, the dLIF provides a good quantitative approximation to the LIF. Outside such regimes, it captures the qualitative dependence of the spiking statistics on parameters. We emphasize that the purpose of the model is not to quantitatively approximate the LIF (which is itself a simplified model). Instead, the dLIF serves as an analytically tractable leaky model that can be used to understand the principal mechanisms that shape correlation transfer.

When $e(t)$ and $i(t)$ are Poisson, the membrane potential $V(t)$ for the dLIF model is a continuous-time Markov process on a discrete state-space, and we can compute the univariate and bivariate spiking statistics exactly (see appendix D). It is hereafter assumed that e(t) and i(t) are Poisson when referring to the dLIF model. The stationary firing rate and CV for the dLIF are derived in closed form in appendix D,

$$r_{out} = \frac{(\hat{q} - 1)^2}{\hat{q}\left((\hat{q}^{-\theta} - 1)\,\hat{q}^{\beta} + \theta(\hat{q} - 1)\right)}\, r_e, \tag{2.6}$$

and

$$\mathrm{CV}^2_{out} = \frac{4(\hat{q}(\theta - \beta + 1) - \theta + \beta)\hat{q}^{\theta+\beta} + \hat{q}^{2\beta} + \hat{q}^{2\theta}(-(\hat{q}^{2\beta} - 4(\hat{q}(\beta - 1) - \beta)\hat{q}^{\beta} - \hat{q}^2\theta + \theta))}{(\hat{q}^{\beta} - \hat{q}^{\theta}(\hat{q}^{\beta} - \hat{q}\theta + \theta))^2}, \tag{2.7}$$

where $\hat{q} = r_e/(r_i + \bar{I}_L)$. Throughout the text, we take $\beta = -2$ and $\theta = 30$. Figure 3 shows that the input-to-output rate curve has the threshold-linear shape that is typical of integrate-and-fire neurons. In the fluctuation-dominated regime, $CV_{out} \approx 1$, while in the drift-dominated regime, CV_{out} is decreased.

We were unable to derive closed-form expressions for the bivariate and time-dependent univariate spiking statistics. However, since the membrane potentials are a Markov process on a discrete state-space, their exact time-dependent distributions can be found by exponentiating their infinitesimal generator matrix, and the stationary distribution is given by the dominant eigenspace of the generator. (These methods are discussed in detail in appendix D, and a suite of Matlab programs that implement these methods can be found online at http://www.mathworks.com/matlabcentral/fileexchange/28686.)

2.7 Memory Timescale of the dLIF Model. The membrane potential of the dLIF model with Poisson inputs is an ergodic Markov process. The infinitesimal generator for such a process has exactly one zero left eigenvalue, and the remaining left eigenvalues have negative real part (Karlin & Taylor, 1975). The nonzero left eigenvalue with the real part nearest to zero, λ_1, determines the timescale at which the membrane potential relaxes to its stationary distribution. In particular, defining $\tau_{mem} = -1/\mathrm{Re}(\lambda_1)$, the distribution relaxes to its steady state exponentially as $e^{-t/\tau_{mem}}$. We use this result in sections 4 and 7 to analyze the asymptotic correlation and estimate the tail of the cross-covariance function for the dLIF model. (See appendix D for a fuller discussion.)

3 Correlations Are Nearly Preserved in Drift-Dominated Regimes

When excitation is stronger than inhibition and leak, the membrane dynamics of a leaky model can be approximated by the PIF (see section 2 and Figure 2). Input to the model neurons, $\mathrm{in}_j(t) = \mathrm{e}_j(t) - \mathrm{i}_j(t)$, $j = 1, 2$, is a sum of excitatory, $\mathrm{e}_j(t)$, and inhibitory, $\mathrm{i}_j(t)$, components. When $r_e - r_i > 0$, the output firing rate of the PIF is positive, with spike count

$$\begin{aligned} N_{\mathrm{out}_j}(t) &= \frac{N_{\mathrm{e}_j}(t) - N_{\mathrm{i}_j}(t) - V_j(t) + V_j(0)}{\theta} \\ &= \frac{1}{\theta} N_{\mathrm{in}_j}(t) + \mathcal{O}(1), \quad j = 1, 2, \end{aligned} \tag{3.1}$$

where $\mathcal{O}(1)$ represents terms bounded in time. Thus, for large t, the input and output spike counts are linearly related.

This implies that $\sigma^2_{out} = \sigma^2_{in}/\theta^2$ and $\gamma_{out} = \gamma_{in}/\theta^2$. The covariance and variance are scaled by the same factor, and therefore the correlation coefficient

is unchanged by a layer of PIFs:

$$\rho_{\text{out}} = \rho_{\text{in}} = \frac{\rho_{\text{ee}}\sigma_{\text{e}}^2 + \rho_{\text{ii}}\sigma_{\text{i}}^2 - 2\rho_{\text{ei}}\sigma_{\text{e}}\sigma_{\text{i}}}{\sigma_{\text{e}}^2 + \sigma_{\text{i}}^2}. \tag{3.2}$$

The fact that $\rho_{\text{out}} = \rho_{\text{in}}$ is valid for a pair of PIFs with arbitrary stationary inputs with positive mean (see appendix B for a detailed proof). Thus, the result does not depend on the assumption of instantaneous postsynaptic potentials and remains true when inputs are modeled as continuous (e.g., white) noise (Vilela & Lindner, 2009). It follows that a threshold mechanism or a threshold-linear f-I curve alone is not enough to reduce correlations.

We conclude that a pair of LIFs in the drift-dominated regime nearly preserves correlations. This conclusion is consistent with previous observations for LIF models driven by correlated, positively biased white noise (de la Rocha et al., 2007; Shea-Brown, Josić, de La Rocha, & Doiron, 2008; Tchumatchenko, Malyshev, Geisel,Volgushev, & Wolf, 2008; Vilela & Lindner, 2009) and is verified for the LIF with discrete postsynaptic potentials in Figure 4. In the drift-dominated regime, output correlations for a pair of LIFs approximately match the theoretical values obtained for PIFs. Outside of this regime, the LIF output correlations are reduced in magnitude. We investigate this reduction of correlations next.

4 Correlations Are Reduced in Fluctuation-Dominated Regimes

When input to the cells is weaker and firing rates lower, correlations are reduced in the output (Stroeve & Gielen, 2001, de la Rocha et al., 2007, Shea-Brown et al., 2008; Tchumatchenko et al., 2008). In this section, we provide a mechanistic explanation of this reduction in correlations, which can be observed in the LIF simulations in Figure 4. Although our explanation applies to a wide class of neuron models, we illustrate the results with the dLIF model described in section 2. This model is simple enough that the output correlation and other quantities of interest can be computed exactly, yet it captures the overall features of correlation transfer in both the drift- and fluctuation-dominated regimes.

The fact that the PIF preserves correlations relies on an asymptotically linear and deterministic relation between the input and output spike counts (see equation 3.1). The same relation holds approximately for the LIF in drift-dominated regimes since leak has a small effect, and the lower boundary of the membrane voltage is visited rarely (see Figure 2).

However, in the fluctuation-dominated regime where spiking is caused by random fluctuations of the membrane potential, the output spike count over large windows depends on the timing of input spikes instead of the input spike count alone. As a result, the relationship between input and output spike counts is stochastic and nonlinear so that equation 3.1

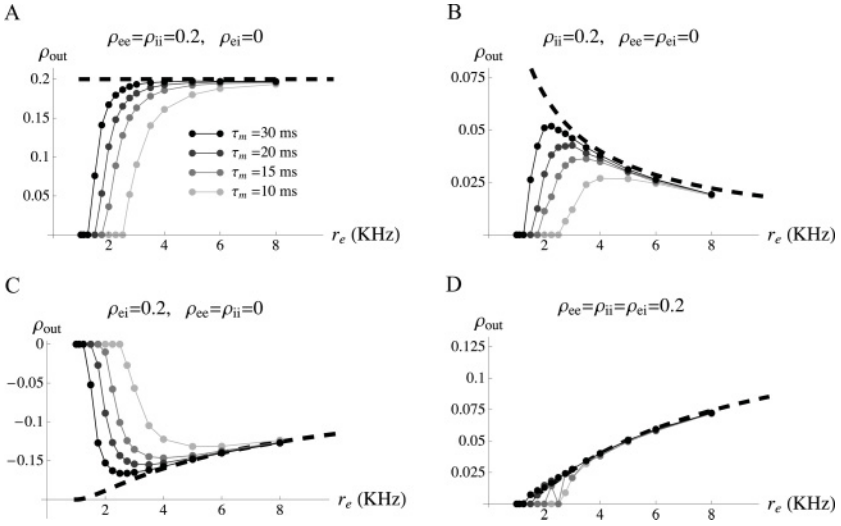

Figure 4: Correlation transfer for the LIF model. In each panel, a set of input correlations, ρ_{ee}, ρ_{ii}, and ρ_{ei} is fixed. Output correlations, ρ_{out}, are shown as functions of the excitatory input rate when $r_i = 1$ KHz. Thick dashed lines represent the output correlation for the PIF (see equation 3.2). Thin solid lines represent output correlation from simulations of the LIF with correlated Poisson inputs. Along each dashed line, the membrane time constant is held fixed and is larger for darker lines (see legend). As the rate of excitation increases relative to inhibition and relative to leak, the LIF is better approximated by the PIF. The output rates for the LIF varied from less than 10^{-3} Hz to 216 Hz. The PIF and LIF agree well (equivalently, correlations are nearly preserved) for moderate firing rates, for example, $|\rho_{LIF} - \rho_{PIF}| \leq 0.1\rho_{PIF}$ when $r_{out} \geq 40$ Hz and $\tau_m = 20$ ms in *A*. Correlation parameters are (A) $\rho_{ee} = \rho_{ii} = 0.2$ and $\rho_{ei} = 0$, (B) $\rho_{ii} = 0.2$ and $\rho_{ee} = \rho_{ei} = 0$, (C) $\rho_{ei} = 0.2$ and $\rho_{ee} = \rho_{ii} = 0$, and (D) $\rho_{ee} = \rho_{ii} = \rho_{ei} = 0.2$. Here, and in all subsequent figures, sample points from simulations are marked with dots, and error bars are not drawn when the standard errors are smaller than the diameter of the dots. Otherwise, error bars have radius of one standard error.

is no longer valid. To understand correlation transfer in the fluctuation-dominated regime, we instead consider the following equation for the output correlation derived in appendix C:

$$\rho_{out} = \frac{CV_{out}^2 + 1}{CV_{out}^2}\left(\frac{E[\tau_1] - E[\tau_1 \mid V_2 \nearrow \theta]}{E[\tau_1]}\right) + \frac{S_{out}}{CV_{out}^2}.$$

Here $E[\tau_1 \mid V_2 \nearrow \theta]$ is the expected time until the next spike in neuron 1 given that neuron 2 has just spiked, and $E[\tau_1] = \left(CV^2 + 1\right)/(2r_{out})$ is

the expected time until the next spike in neuron 1 starting from an arbitrary initial time (referred to in Cox, 1962, as the expected recurrence time).

When the excitatory inputs are correlated synchronously ($S_{e_1e_2} > 0$), there is a nonzero probability of an exactly synchronous spike in neurons 1 and 2. This leads to positive values of S_{out} and thereby increases ρ_{out}. However, in the fluctuation-dominated regime, S_{out} is small and can be ignored (see the Figure 6 inset). Also, in this regime, firing is approximately Poissonian so that $\text{CV}^2_{\text{out}} \approx 1$ (see Figure 3B) and $(\text{CV}^2_{\text{out}} + 1)/\text{CV}^2_{\text{out}} \approx 2$. Therefore, in the fluctuation-dominated regime, changes in ρ_{out} are dominated by the "memory,"

$$M = \frac{E[\tau_1] - E[\tau_1 \mid V_2 \nearrow \theta]}{E[\tau_1]},$$

which quantifies the relative impact of a spike in neuron 2 on the time until the next spike in neuron 1. In particular, $\rho_{\text{out}} \approx 2M$ in the fluctuation-dominated regime.

When V_1 and V_2 are independent, $E[\tau_1 \mid V_2 \nearrow \theta] = E[\tau_1]$ and $S_{\text{out}} = 0$ so that $\rho_{\text{out}} = 0$. When V_1 and V_2 are positively correlated, conditioning on V_2 being at threshold increases the probability that V_1 is near threshold. This decreases the expected time for V_1 to reach threshold, yielding $E[\tau_1 \mid V_2 \nearrow \theta] \leq E[\tau_1]$ and a positive value of M. A positive value of M implies a positive value of ρ_{out} since $S_{\text{out}} \geq 0$. Similarly, when V_1 and V_2 are negatively correlated, the expected time until V_1 reaches threshold is lengthened by conditioning on V_2 being at threshold. Therefore, $E[\tau_1 \mid V_2 \nearrow \theta] \geq E[\tau_1]$, resulting in negative output correlations when S_{out} is sufficiently small.

When excitation is weak in relation to inhibition and leak, firing is due to rare excursions of the membrane potential across threshold (Paninski, 2006; Ringach & Malone, 2007). The stationary distribution of the membrane potentials is concentrated near rest, but conditioning on a spike in neuron 2 pushes the distribution of V_1 closer to threshold. The distribution of V_1 then relaxes back to its stationary distribution. The timescale of this relaxation is given by the memory timescale, τ_{mem} (see section 2). In Figure 5A, we show that the memory timescale is much faster than the spiking timescale ($\tau_{\text{mem}} \ll E[\tau_1]$) in the fluctuation-dominated regime. This is due to the fact that the spiking dynamics are much slower than the subthreshold dynamics in this regime. The result of this effect is illustrated in Figure 5B: the distribution of V_1 settles to its stationary state long before the next spike. Neuron 1 effectively forgets the effects of the spike in neuron 2 before it has a chance to spike (Knight, 1972). Therefore, a spike in cell 2 has a small impact on the waiting time to the next spike in cell 1 and the output spike trains are nearly independent. As a result, $E[\tau_1] \approx E[\tau_1 \mid V_2 \nearrow \theta]$ (the arrows in Figure 5B are close together) so that $M \approx 0$, and therefore $\rho_{\text{out}} \approx 0$.

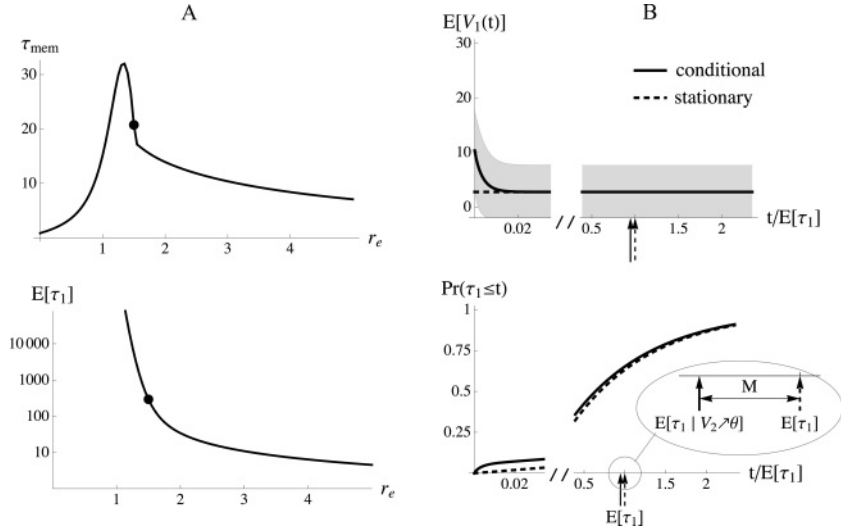

Figure 5: Forgetfulness of cells in the fluctuation-dominated regime. (A) The memory timescale (τ_{mem}) and the spiking timescale ($E[\tau_1]$) plotted as a function of r_e when $r_i = 1$ and $\bar{I}_L = 0.5$. The filled circles indicate the boundary between the fluctuation and drift-dominated regimes: $r_e = r_i + \bar{I}_L$. (B) Top: The mean membrane potential of neuron 1 conditioned on a spike in neuron 2 at time $t = 0$ (solid line). The shaded region represents the mass within one standard deviation of the mean, and the dashed line indicates the stationary mean. Bottom: The cumulative probability distribution of the waiting time, τ_1, of the next spike in neuron 1, conditioned on a spike in neuron two at time $t = 0$ (solid line) and in the stationary case (dashed line). Arrows indicate the expected value of τ_1 in the stationary (solid) and conditional (dashed) cases. The distance between the two arrows is $M = (E[\tau_1] - E[\tau_1 | V_2 \nearrow \theta])/E[\tau_1]$. Parameters in B are $r_e = 1.25$, $r_i = 1$, $\bar{I}_L = 0.5$, $\rho_{ee} = \rho_{ii} = 0.5$ and $\rho_{ei} = 0$.

As r_e increases toward the drift-dominated regime, conditioning on V_2 being at threshold has an increasing relative impact on the expected waiting time until V_1 spikes, and as a result, $|M|$ increases (see Figure 6). Since $|M|$ dominates in equation 2.4, $|\rho_{\text{out}}|$ also increases as the drift-dominated regime is approached. Inside the drift-dominated regime, $\rho_{\text{out}} \approx \rho_{\text{in}}$, as discussed previously. The dependence of ρ_{out} on the level of excitation is illustrated for the dLIF in Figure 7 and is consistent with the LIF simulations in Figure 4.

The reduction of dependencies between the output spike trains in the fluctuation-dominated regime does not depend on our choice of the Pearson correlation coefficient as a measure. When firing is rare, output spike trains become nearly independent. Thus, any reasonable measure of dependence

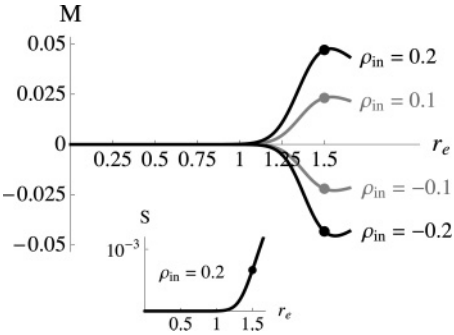

Figure 6: Dependence of M on r_e for the dLIF model. Here $\rho_{ee} = \rho_{ii} = \rho_{in}$ and $\rho_{ei} = 0$ for lines in the upper half. For lines in the lower half, $\rho_{ee} = \rho_{ii} = 0$, and ρ_{ei} is chosen so that $\rho_{in} = -0.2$ and -0.1, respectively. For all four lines, $r_i = 1$ and $\bar{I}_L = 0.5$ are fixed (so that r_e and $\bar{I}_L$ are given in units of r_i). The inset shows the output synchrony, S_{out}, as a function of r_e with $\rho_{ee} = \rho_{ii} = 0.2$ and $\rho_{ei} = 0$. Filled circles indicate the values for which $r_e = r_i + \bar{I}_L = 1.5$, which defines the boundary between the fluctuation and drift-dominated regimes. When $r_e \ll r_i + \bar{I}_L$, M is approximately 0. As the cell approaches the drift-dominated regime, $|M|$ increases. Interestingly, $|M|$ decreases with r_e in the drift-dominated regime. However, in this regime, S is no longer negligible and CV_{out} decreases with r_e (see the inset and Figure 3B), so that the value of M alone is no longer a good indicator of the value of ρ_{out}.

between output spike trains tends to zero in the fluctuation-dominated limit. We revisit this observation in section 9.

Some combinations of the correlation parameters can lead to nonmonotonic behavior of ρ_{out} with respect to r_e. For instance, in Figure 7B, $\rho_{in} > 0$ so that ρ_{out} initially increases with r_e from 0 toward $\rho_{in} > 0$. However, as r_e continues to grow, uncorrelated excitation dominates and ρ_{out} decreases toward $\rho_{in} \approx \rho_{ee} = 0$. The opposite occurs in Figure 7C: correlation initially decreases from 0 toward $\rho_{in} < 0$ and then increases toward $\rho_{ee} = 0$.

A nonmonotonic relationship between r_e and ρ_{out} yields a nonmonotonic relationship between r_{out} and ρ_{out} since r_{out} increases with r_e. Therefore, correlations do not necessarily increase with firing rate (de la Rocha et al., 2007). Such mechanisms could underlie the attention-induced decreases in correlations accompanied by increases in firing rates (Cohen & Maunsell, 2009). This result is not necessarily in opposition to the central result in de la Rocha et al. (2007), which implies an increase in the correlation susceptibility, ρ_{out}/ρ_{in}, with respect to firing rates. In Figures 7A to 7C, the correlation susceptibility increases with r_{out}. However in Figure 7D, $\rho_{in} = 0$ when $r_e = r_i$, but $\rho_{out} > 0$ so that the correlation susceptibility is undefined at this point. This phenomenon is explored further in section 8.1.

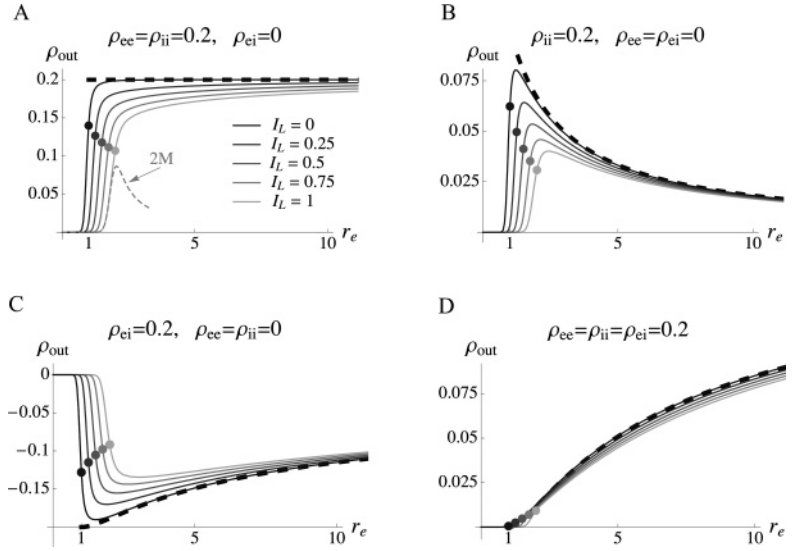

Figure 7: Correlation transfer for the dLIF model. The output correlation as a function of the excitatory input rate, r_e, for different combinations of the correlations parameters, ρ_{ee}, ρ_{ii}, ρ_{ei}, and the mean leak current, $\bar{I}_L$. We fixed $r_i = 1$ and varied r_e and $\bar{I}_L$; thus, r_e and $\bar{I}_L$ are given in units of r_i. The solid lines represent the output correlations for the dLIF, and the dashed lines represent values for the PIF (equivalently the input correlation, ρ_{in}). The mean leak current, $\bar{I}_L$, decreases with the darkness of the solid lines. The darkest solid line is obtained by setting $\bar{I}_L = 0$, eliminating the leak current altogether. In this case, the dLIF differs from the PIF only by the presence of a lower reflecting barrier at β. When $r_e < r_i$, this lower barrier has a decorrelating effect. When excitation is stronger, the lower barrier has an insignificant effect on correlations since it is visited rarely. The filled circles indicate the boundary between the drift- and fluctuation-dominated regimes, $r_e = r_i i + \bar{I}_L$. The correlation parameters are (A) $\rho_{ee} = \rho_{ii} = 0.2$ and $\rho_{ei} = 0$, (B) $\rho_{ii} = 0.2$ and $\rho_{ee} = \rho_{ei} = 0$, (C) $\rho_{ei} = 0.2$ and $\rho_{ee} = \rho_{ii} = 0$, and (D) $\rho_{ee} = \rho_{ii} = \rho_{ei} = 0.2$.

5 Synaptic Variability Reduces Correlations

Synapses can have a range of efficacies, and spikes in presynaptic neurons can elicit a variety of postsynaptic response amplitudes. Furthermore, synaptic failure and random response amplitudes result in variability at the level of single synapses. Release probabilities at a synapse range between less than 0.1 and up to 0.9 (Allen & Stevens, 1994; Thomson, 2000), and the magnitude of the postsynaptic response, evoked by the same cell, can vary with a CV from .25 to 1.5 (Mason, Nicoll, & Stratford, 1991; Hessler, Shirke, & Malinow, 1993; Brémaud, West, & Thomson, 2007).

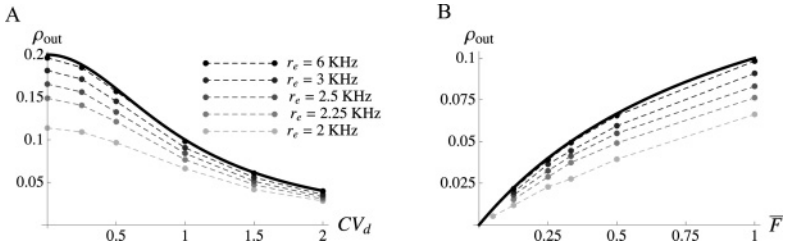

Figure 8: Effects of synaptic variability on correlation transfer. Solid lines indicate theoretical values for a pair of PIFs (see equation 5.1), and thin dashed lines were obtained from simulations of a pair of LIFs. For the LIF simulations, $r_{\text{i}} = 1$ KHz and $\tau_m = 20$ ms are fixed, and the excitatory input rate, r_{e}, increases with the darkness of the lines (see legend). The correlation parameters are $\rho_{\text{ee}} = \rho_{\text{ii}} = 0.2$ and $\rho_{\text{ei}} = 0$. Inputs are renewal with gamma-distributed ISIs (see appendix A) and postsynaptic amplitudes are random, with peak values drawn independently from a gamma distribution with mean 1 and coefficient of variation CV_d. In the drift-dominated limit, the PIF accurately approximates the LIF (see the darkest dotted lines). Outside this regime (the lighter lines), correlations are reduced but obey the same dependence on the parameters. (A) The input Fano factor, $\overline{F}$, is fixed at unity (inputs are Poisson), and the magnitude of synaptic noise, CV_d, is varie. (B) The degree of synaptic variability is fixed at $\text{CV}_d = 1$, and $\overline{F}$ is varied.

To model synaptic variability, assume that an excitatory (inhibitory) spike at time t_{e}^k (t_{i}^k), causes a random "jump" d_{e}^k (d_{i}^k) in the membrane potential of the postsynaptic cell. Assume that the jumps are drawn independently from a distribution with mean $\overline{d}_{\text{e}}$ ($\overline{d}_{\text{i}}$) and variance $\sigma_{d_{\text{e}}}^2$ ($\sigma_{d_{\text{i}}}^2$). For simplicity, we let $\overline{d}_{\text{e}} = \overline{d}_{\text{i}} = \overline{d}$ and $\sigma_{d_{\text{e}}}^2 = \sigma_{d_{\text{i}}}^2 = \sigma_d^2$ (more general results are given in appendix E.1).

Synaptic noise adds stochasticity to the relationship between input and output spike counts given for the PIF by equation 3.1, but randomness is introduced only at each input spike. As a result, the variance is increased by an amount that depends on the input rates. In particular, for the PIF, $\sigma_{\text{out}}^2 = (\sigma_{\text{in}}^2 + \text{CV}_d{}^2(r_{\text{e}} + r_{\text{i}}))/\hat{\theta}^2$ where $\hat{\theta} = \theta/\overline{d}$ is the average number of excitatory kicks needed to reach threshold and $\text{CV}_d = \sigma_d/\overline{d}$. Since synaptic noise was assumed to be independent, the covariance of the outputs is not changed by the noisiness of the synapses, $\gamma_{\text{out}} = \gamma_{\text{in}}/\hat{\theta}^2$. Correlations are therefore reduced as (see appendix E.1)

$$\rho_{\text{out}} = \left(\frac{\overline{F}}{\overline{F} + \text{CV}_d^2} \right) \rho_{\text{in}}, \tag{5.1}$$

where $\overline{F} = (F_{\text{e}} r_{\text{e}} + F_{\text{i}} r_{\text{i}})/(r_{\text{e}} + r_{\text{i}})$ is the weighted average of the excitatory and inhibitory input Fano factors. The decrease in correlations due to synaptic noise is illustrated in Figure 8A. Interestingly an increase in the

randomness of the input, as measured by $\overline{F}$, will increase the output correlation, but only in the presence of synaptic noise. This effect is illustrated in Figure 8B.

Synaptic failure can be modeled by assuming that d_{e}^k and d_{i}^k are binary random variables, in which case $\mathrm{CV}_d^2 = (1-p)/p$, where p is the probability of release. For example, when inputs are Poisson ($\overline{F} = 1$), $\rho_{\mathrm{out}} = p$ for the PIF model. Hence, ρ_{out} decreases with an increase in the probability of synaptic failure. When p is small (Allen & Stevens, 1994; Thomson, 2000), correlations are significantly reduced by synaptic failure.

Combining the effects of synaptic failure and variable postsynaptic amplitudes, we obtain

$$\rho_{\mathrm{out}} = \left(\frac{p\,\overline{F}}{p\,\overline{F} + (1-p) + \mathrm{CV}_d^2} \right) \rho_{\mathrm{in}}, \tag{5.2}$$

where we have assumed that a proportion p of the inputs successfully elicits a response, and the amplitudes of the successful synaptic responses are variable with a CV of CV_d. Realistic choices of parameters yield dramatic reductions in correlations. For example, taking $p = 0.5$, $\mathrm{CV}_d = 1$, and $\mathrm{CV}_{\mathrm{e}} = \mathrm{CV}_{\mathrm{i}} = 0.6$ (where $\overline{F} = \mathrm{CV}_{\mathrm{e}}^2$), correlations are reduced by nearly an order of magnitude by the PIF ($\rho_{\mathrm{out}} = 0.107\rho_{\mathrm{in}}$). Correlations are reduced even further by leaky models, especially in the fluctuation-dominated regime. In Figure 9, we illustrate the effects of synaptic variability on correlations in a simple population model.

Because the release probability and PSP amplitude are dependent on input statistics (Czubayko & Plenz, 2002), the independence assumptions made in this section can be taken only as a first approximation. However, the model can be extended to take such dependencies into account.

6 Effect of Coupling on Correlations

Recurrent connections are common in many parts of the central nervous system and may play an important role in information processing (Gawne & Richmond, 1993; Kisvárday, Tóth, Rausch, & Eysel, 1997; Gibson, Beierlein, & Connors, 1999; Lamme & Roelfsema, 2000; Oswald, Doiron, Rinzel, & Reyes, 2009). Synaptic coupling or gap junctions can actively modulate the transfer of correlated inputs (Schneider, Lewis, & Rinzel, 2006; Ly & Ermentrout, 2009), and thus affect the information carried by a population of cells (Gutnisky & Dragoi, 2008; Josić, Shea-Brown, Doiron, & de la Rocha, 2009).

To model recurrent coupling between two cells, suppose that an action potential in one cell instantaneously raises the membrane potential of the other. We consider a pair of identical, reciprocally coupled cells here, but more general results are given in appendix E.2. The jump in membrane potential, c, due to reciprocal coupling is assumed to be smaller than θ.

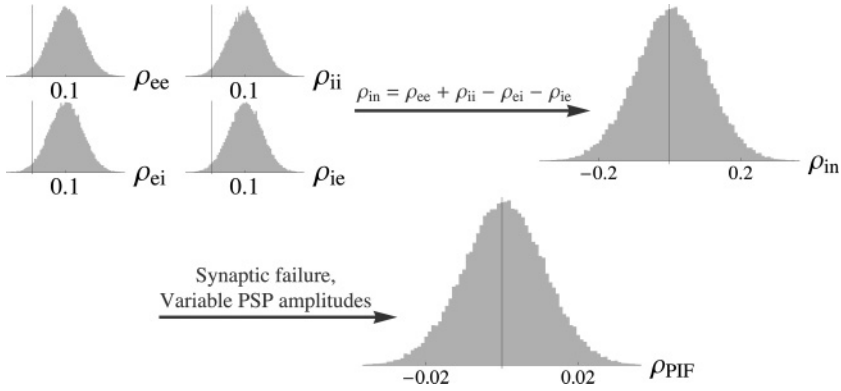

Figure 9: Correlations are dramatically reduced by unreliable synapses. The input population has excitatory-to-excitatory (ee), inhibitory-to-inhibitory (ii), and excitatory-to-inhibitory (ei) correlations distributed according to a normal distribution with a mean of 0.1 and a standard deviation of 0.05. Assuming homogeneous rates and balanced excitation and inhibition, the input correlations to downstream cells are normally distributed with a mean of 0 (the ei correlations "cancel" with the ee and ii correlations) and a standard deviation of $2 \times 0.05 = 0.1$ (the variances sum). However, realistic levels of synaptic failure, variability of synaptic amplitudes, and non-Poisson input statistics ($\mathrm{CV}_d = 1$, $p = 0.5$, $\mathrm{CV}_e = \mathrm{CV}_i = 0.6$, $\overline{F} = \mathrm{CV}_e^2$; see section 5) decrease output correlations for the PIF by almost an order of magnitude, $\mathrm{std}(\rho_{\mathrm{PIF}}) = 0.0107$. Correlations are reduced even further for leaky models, especially in fluctuation-dominated regimes (see section 4 and Figure 8).

The membrane potentials of a pair of coupled PIFs are described by the coupled differential equations,

$$dV_1 = \mathrm{in}_1(t)\,dt + c\,\mathrm{out}_2(t)\,dt, \quad dV_2 = \mathrm{in}_2(t)\,dt + c\,\mathrm{out}_1(t)\,dt,$$

with the usual threshold and reset boundary conditions. The analog of equation 3.1 in this case is a coupled set of linear equations. Their solution can be used to compute the output variance and covariance for the PIF (see appendix E.2),

$$\sigma^2_{\mathrm{out}} = \frac{\sigma^2_{\mathrm{in}}}{(\theta^2 - c^2)^2}\left[(\theta^2 + c^2) + 2c\theta\rho_{\mathrm{in}}\right], \quad \text{and}$$

$$\gamma_{\mathrm{out}} = \frac{\gamma_{\mathrm{in}}}{(\theta^2 - c^2)^2}\left[(\theta^2 + c^2) + \frac{2c\theta}{\rho_{\mathrm{in}}}\right].$$

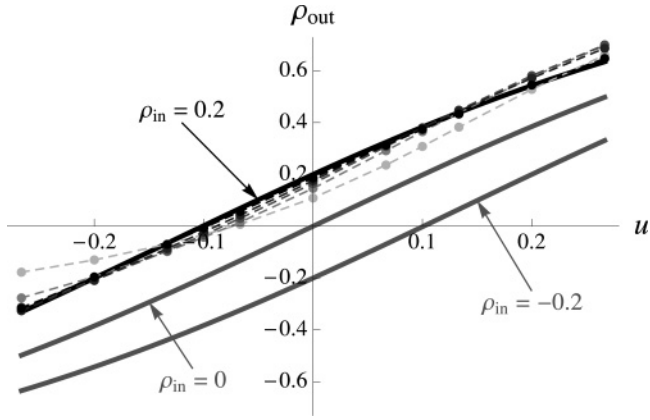

Figure 10: Effect of coupling on correlation transfer. Solid lines indicate theoretical values for a pair of PIFs (see equation 6.1), and thin dashed lines were obtained from simulations of a pair of LIFs with $\rho_{ee} = \rho_{ii} = 0.2$, $\rho_{ei} = 0$ so that $\rho_{in} = 0.2$. Parameters are the same as in Figure 8, except that inputs are strictly Poisson and synapses are not random.

Since $|\rho_{in}| < 1$, it follows that coupling has a larger effect on the covariance than on the variance. This can be understood by noting that coupling affects the covariance directly and affects the variance only indirectly (Rangan, 2009): when neuron 1 spikes, the membrane potential of neuron 2 (and therefore the timing of its spikes) is affected directly due to coupling. However, the effect on neuron 1 itself is indirect: a spike in neuron 1 affects the propensity of neuron 2 to spike, which in turn affects the timing of spikes in neuron 1.

The output correlation is

$$\rho_{out} = \frac{(1+u^2)\rho_{in} + 2u}{(1+u^2) + 2u\rho_{in}}, \tag{6.1}$$

where $u = c/\theta < 1$ is synaptic amplitude relative to the distance from reset to threshold and measures the strength of the coupling. If the coupling is not too strong, then to first order in u, $\rho_{out} = \rho_{in} + 2(1-\rho_{in}^2)u + \mathcal{O}\left(u^2\right)$. Figure 10 illustrates the dependence of ρ_{out} on u when ρ_{in} is fixed. Not surprisingly, excitatory coupling ($u > 0$) increases correlations, and inhibitory coupling ($u < 0$) decreases correlations. Frequently, the amplitude of a single PSP is much smaller than the distance from reset to threshold (i.e., u is small), and therefore the effect of coupling on correlations is small.

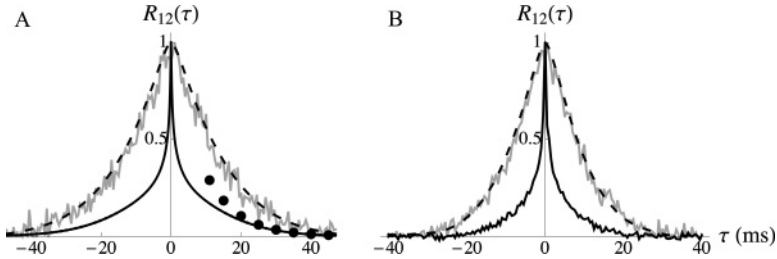

Figure 11: Output cross-covariance functions. The output cross-covariance function when inputs are delta correlated (black lines) decays with a timescale of τ_{mem} (black dots follow $e^{-\tau/\tau_{\text{mem}}}$). The gray lines show the output cross-covariance when the input cross-covariance is a double exponential, $(\gamma_{\text{in}}/2)e^{-|\tau|/5}$, instead of a delta function. The dashed line was obtained by convolving the input cross-covariance function with the output cross-covariance function obtained in the delta-correlated case. (A) Cross-covariance functions for the dLIF with $r_{\text{e}} = 3$, $r_{\text{i}} = 2$, $\rho_{\text{ee}} = \rho_{\text{ii}} = 0.2$, $\rho_{\text{ei}} = 0$, and $\bar{I}_L = 0.877$ were chosen so that the output rate ($r_{\text{out}} = 8.4$ Hz) matches the LIF simulations in *B*. The black solid and dashed lines were obtained exactly, without simulations. The gray line is from simulations. (B) Cross-covariance function from LIF simulations with the same parameters as in *A* and $\tau_m = 20$ ms. In both plots, inputs are Poisson (see appendix A), and cross-covariance functions are normalized to have a peak value of 1.

7 Cross-Covariance Functions and the Timescale of Correlations

So far we have focused on the magnitude of correlations over asymptotically large windows (see the definition of ρ_{ab} in section 2). However, the timescale over which correlations occur is often of interest in both theoretical and experimental studies (Maršálek, Koch, & Maunsell, 1997; Brody, 1999; Kohn & Smith, 2005; Moreno-Bote & Parga, 2006; Ostojić, Brunel, & Hakim, 2009). We provide a brief discussion of the topic here. A full treatment of the topic will be addressed in a forthcoming publication.

The timescale over which two spike trains are correlated can be measured by their auto- and cross-covariance functions, which can be computed exactly for the dLIF model (see section 2 and appendix D). When inputs are delta correlated, the tail of the cross-covariance function, $R_{12}(\tau)$, decays exponentially as $\tau \to \infty$. The timescale of this decay is given by the memory timescale, τ_{mem}, of neuron 2 (see the dotted line in Figure 11A) and the $\tau \to -\infty$ tail decays as the memory timescale of neuron 1.

To address the question of how correlation timescales are transferred, the timescale of input correlations must be taken into account. So far, we have concentrated on "delta-correlated" inputs—inputs whose cross-covariance is a delta function. In particular, the analysis of the dLIF model relied on this

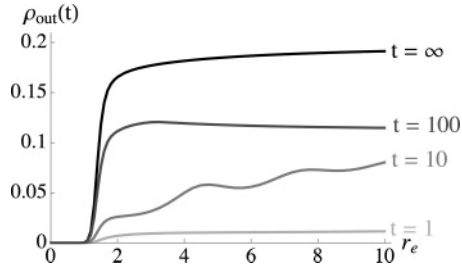

Figure 12: Correlation over finite windows. The output spike count correlation, $\rho_{out}(t)$, over a window of size t, plotted as a function of the input excitatory rate, r_e for various values of t. Correlations are smaller for smaller window sizes but obey the same general dependence on r_e.

assumption. In Figure 11, we show that the cross-covariance obtained from delta-correlated inputs can be used as an impulse response function for the transfer of cross-covariance functions. The output cross-covariance is well approximated by convolving the input cross-covariance with the output cross-covariance obtained with delta-correlated inputs (compare the gray and dashed lines in Figure 11). Thus, the timescale of output correlations is given by $\tau_{out} = \max\{\tau_{mem}, \tau_{in}\}$, where τ_{in} and τ_{out} are the timescales of the input and output cross-covariance functions, respectively. Figure 11 also illustrates that the cross-covariance functions for the dLIF match those for the LIF qualitatively when the two models have identical input parameters and $\bar{I}_L$ is chosen so that the rates of the two models are matched.

The spike count correlations over finite windows can be computed from the auto- and cross-covariance functions (see equation 2.1). Correlations are smaller for smaller window sizes for an LIF model with white noise inputs (Shea-Brown et al., 2008). The dependence of output correlations on window sizes is illustrated in Figure 12 and will be discussed in the authors' forthcoming work.

8 Comparison of Results with Other Models

8.1 Comparison with a White Noise Gaussian Model. In Figure 13A, we compare the analytical results for the dLIF and simulations of the LIF with Poisson inputs to a linear response approximation of the LIF with gaussian white noise inputs, as described by de la Rocha et al. (2007). The models exhibit the same qualitative dependence on r_{out}, but the dLIF differs from the LIF quantitatively to some extent. Both models are caricatures of actual neurons, and neither should be expected to agree quantitatively with actual recordings. The dLIF has the advantage of being more amenable to analysis and simpler to understand mechanistically. We next describe a regime where the dLIF differs from gaussian models even qualitatively.

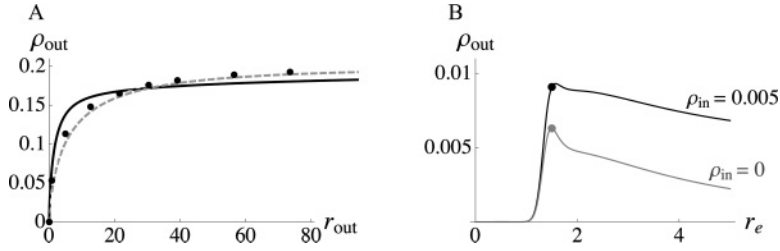

Figure 13: Comparing the dLIF with a gaussian model. (A) Output correlation plotted as a function of output rate for three models: analytical results for the dLIF (solid black line), simulations of an LIF with Poisson inputs (black dots), and a linear response approximation to an LIF with gaussian white noise input (gray dashed line). For the dLIF and LIF with Poisson inputs, the input parameters are as in Figures 4A and 7A with $\tau_m = 20$ ms and $\bar{I}_L = 0.5$. The white noise inputs for the gray dashed line have bias $\mu = r_e - r_i$, variance $\sigma^2 = r_e + r_i$, and correlation $\rho_{in} = 0.2$. (B) Results are from the dLIF model with $r_i = 1$, $\bar{I}_L = 0.5$, $\rho_{ee} = 0.5$, and $\rho_{ii} = 0.5$ fixed. The filled circles indicate the boundary between the drift and fluctuation-dominated regimes, $r_e = r_i i + \bar{I}_L$. As r_e changes, ρ_{ei} is varied so that $\rho_{in} = 0$ and $\rho_{in} = 0.005$, respectively. Output correlations are positive even when $\rho_{in} = 0$. When $\rho_{in} = 0.005$, correlations can double from input to output. Gaussian models cannot exhibit such increases in correlations.

When $2\rho_{ei}\sqrt{r_e e r_i} = \rho_{ee} r_e + \rho_{ii} r_i$, the correlation between the total input currents, ρ_{in}, is zero. In such cases, output correlations for the dLIF are positive but very small— about two orders of magnitude smaller than ρ_{ee} and ρ_{ii} (see Figure 13B). Note that small correlations on this scale have the potential to have a significant impact on coding and downstream activity when the output from several neurons is pooled (Zohary et al., 1994; Renart et al., 2010; Rosenbaum et al., 2010). This might explain why large correlations are observed in deeper layers of feedforward networks even when excitation and inhibition are balanced (Litvak, Sompolinsky, Segev, & Abeles, 2003; Rosenbaum et al., 2010).

Integrate-and-fire models are able to transfer uncorrelated input currents to correlated outputs because uncorrelated input currents are not necessarily independent. Since the integrate-and-fire filter is nonlinear, it is possible for moments to "mix" so that higher-order input correlations are transferred to second-order output correlations. This phenomenon cannot be observed when inputs are modeled by gaussian processes, since uncorrelated gaussian processes are necessarily independent. Furthermore, when $2\rho_{ei}\sqrt{r_e r_i} \approx \rho_{ee} r_e + \rho_{ii} r_i$ correlations nearly cancel, and $\rho_{in} \approx 0$. In such cases, it is possible that $|\rho_{out}| > |\rho_{in}| > 0$ for the dLIF model (see Figure 13B). This would again be impossible if inputs were modeled using gaussian processes (Lancaster, 1957).

8.2 Comparison with a Conductance-Based Model. We now compare the results above to simulations of a conductance-based integrate-and-fire model (Dayan & Abbott, 2001) similar to the model used in Salinas and Sejnowski (2000). This type of model can accurately capture the statistics of a variety of neuronal responses (Kobayashi, Tsubo, & Shinomoto, 2009). The subthreshold potential obeys the differential equation

$$C_m \dot{V} = -g_L(V - E_L) - g_{AMPA}(t)(V - E_{AMPA}) - g_{GABA}(t)(V - E_{Cl}),$$

where $g_{AMPA}(t) = (e * epsc)(t)$ and $g_{GABA}(t) = (\mathrm{i} * ipsc)(t)$ are convolutions of the excitatory and inhibitory inputs with postsynaptic conductance kernels. The excitatory (AMPA) postsynaptic conductances were modeled as exponential functions with time constant τ_{AMPA} and peak value $\bar{g}_{AMPA}$,

$$epsc(t) = \bar{g}_{AMPA} e^{-t/\tau_{AMPA}},$$

and the inhibitory (GABA) postsynaptic conductance are double exponentials,

$$ipsc(t) = \frac{\bar{g}_{GABA}}{D}\left(e^{-t/\tau^{(1)}_{GABA}} - e^{-t/\tau^{(2)}_{GABA}}\right),$$

where D is a constant chosen so that $\bar{g}_{GABA}$ is the maximum value of $ipsc(t)$. When the cell crosses threshold, V_θ, a spike is produced, and the potential is reset to E_L, where it is held for a refractory period, τ_{ref}.

The parameters used in the simulations are $E_L = -60$ mV, $E_{AMPA} = 0$, $E_{Cl} = -62$ mV, $V_\theta = -54$ mV, $\tau_m = 20$ ms, $\tau_{AMPA} = 5$ ms, $\tau^{(1)}_{GABA} = 5.6$ ms, $\tau^{(2)}_{GABA} = .285$ ms, $\tau_{\mathrm{ref}} = 2$ ms (compare to parameters in Salinas & Sejnowski, 2000). In Figures 15 and 16, $g_L = C_m/(20\,\mathrm{ms})$ is fixed to obtain a membrane time constant of $\tau_m = 20$ ms. For the simulations in Figure 14, we used several different values of g_L. For all simulations, we, set $\bar{g}_{AMPA} = C_m/(909\,\mathrm{ms})$ so that 30 synchronous excitatory input spikes are required to bring the cell from reset to threshold, in accordance with our choice of $\theta = 30$ for the current-based models (see section 2). We then set $\bar{g}_{GABA} = 10.3215 g_{AMPA}$ so that an inhibitory postsynaptic potential is about twice the size of an excitatory postsynaptic potential when the membrane potential is halfway between rest and threshold.

Figures 14, 15, and 16 show that the conductance-based model transfers correlations in accordance with the theory developed above and illustrated in Figures 4, 7, 8, and 10. However, in Figure 14 the magnitude of correlations begins to decay with r_{e} when r_{e} gets large. This is consistent with Shea-Brown et al. (2008) where such a decrease in correlations is attributed to the refractory period. The effect is significant only when r_{out} is on the same order as $1/\tau_{\mathrm{ref}}$. To illustrate this point, we plotted the correlation when $\tau_{\mathrm{ref}} = 0$ and

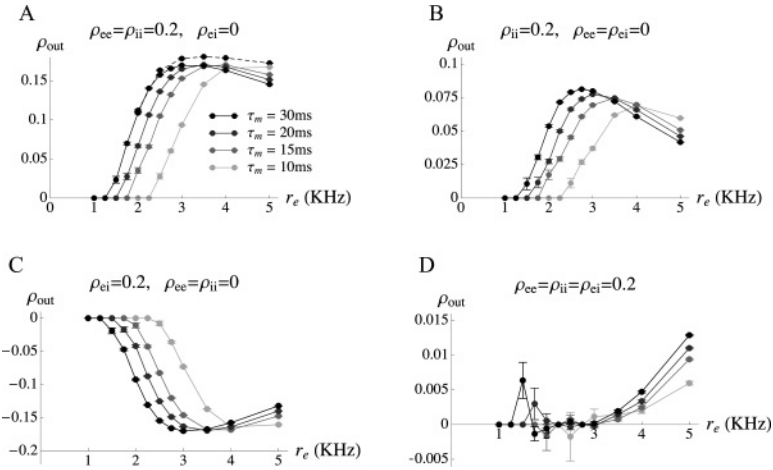

Figure 14: Output correlation as a function of r_e in a conductance-based model. Results from Figures 4 and 7 are reproduced with a conductance-based model. Here, r_e and $\tau_m = C_m/g_L$ are varied, while $r = 1$ KHz is fixed. The membrane time constant, τ_m, is varied by changing g_L and keeping C_m fixed, so that synaptic conductances are not affected. Inputs are correlated Poisson processes. Output rates varied from less than .01 Hz to 130 Hz. For the dashed line in A, we set $\tau_{ref} = 0$ and $\tau_m = 30$ ms to illustrate the effect of a refractory period. Correlations in the inputs are (A) $\rho_{ee} = \rho_{ii} = 0.2$ and $\rho_{ei} = 0$, (B) $\rho_{ii} = 0.2$ and $\rho_{ee} = \rho_{ei} = 0$, (C) $\rho_{ei} = 0.2$ and $\rho_{ee} = \rho_{ii} = 0$, and (D) $\rho_{ee} = \rho_{ii} = \rho_{ei} = 0.2$.

$\tau_m = 30$ ms as a dashed line in Figure 14 (compare to the darkest solid line). The presence of a refractory period causes noticeable decorrelation only once $r_e \geq 3$ KHz, at which point $r_{out} \approx 60$ Hz.

We also observe that correlations are generally smaller in magnitude for the conductance-based model than for the current-based models considered above. This may be a consequence of the fact that the model has more sources of nonlinearity than the current-based models. Another potential explanation is that the effective membrane time constant is reduced when inputs are stronger (Brunel, Chance, Fourcaud, & Abbott, 2001; Kuhn, Aertsen, & Rotter, 2004) so that excitation cannot significantly outweigh the "effective leak."

9 Discussion

We used simplified random walk models of neural dynamics to investigate correlation transfer in a variety of settings and verified that more realistic models obey the same trends. We found that correlations are well preserved in drift-dominated regimes when synaptic variability is not taken into

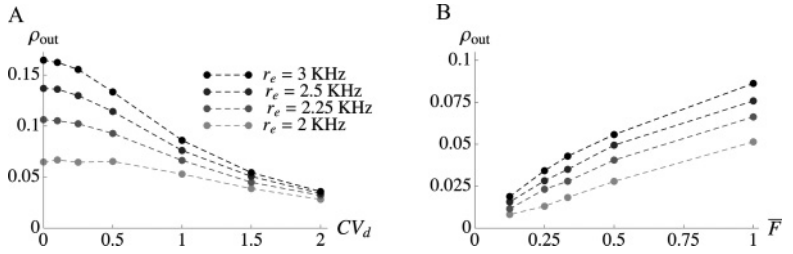

Figure 15: Effects of synaptic variability on correlation transfer in a conductance-based model. Results in Figure 8 are reproduced. Parameters $r_i = 1$ KHz and $\tau_m = 20$ ms are fixed, and the excitatory input rate, r_e, increases with the darkness of the lines (see legend). The input correlation parameters are $\rho_{ee} = \rho_{ii} = 0.2$ and $\rho_{ei} = 0$. Inputs are renewal with gamma distributed ISIs (see appendix A), and EPSCs are random, with peak values drawn independently from a gamma distribution with mean $\bar{g}_{AMPA}$ and coefficient of variation CV_d. (A) The input Fano factor, $F_e = F_i = \overline{F}_{in} = 1$, is fixed, and CV_d is varied. (B) The synaptic variability, $CV_d = 1$, is fixed, and $F_e = F_i = \overline{F}$ is varied.

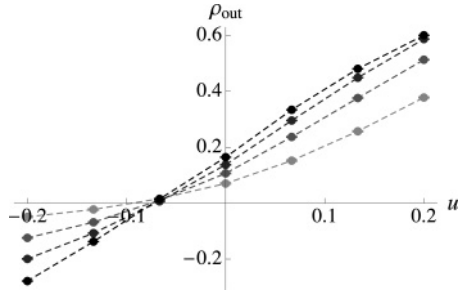

Figure 16: Effects of coupling on correlation transfer in a conductance-based model. Results in Figure 10 are reproduced. Parameters are the same as in Figure 15, except inputs are strictly Poisson and synapses are deterministic. When $u > 0$, a spike in one neuron adds a PSC to the AMPA conductance of the second. The peak value of the EPSC is given by $u \cdot \bar{g}_{AMPA}/30$ so that the corresponding PSP amplitude is roughly a proportion u of the distance from rest to threshold. When $u < 0$ spikes in one neuron, add a PSC with peak value $u \cdot \bar{g}_{GABA}/60$ to the GABA conductance of the other to obtain a similar scaling.

account. However, correlations are reduced outside the drift-dominated regime and reduced further in the presence of synaptic variability and synaptic failure. Positive coupling can increase correlated variability, but only to moderate levels, unless the coupling is strong.

Recent experimental and theoretical studies (Hertz, 2010; Renart et al., 2010) suggest that recurrent network dynamics can modulate correlations

to prevent the potential blowup of correlations observed in a feedforward setting (Reyes, 2003; Rosenbaum et al., 2010). These studies agree with in vivo recordings that show small (Ecker et al., 2010; Renart et al., 2010) or moderate (Zohary et al., 1994) correlations between cells. We showed that correlations are also strongly modulated by dynamics at the cellular level. The correlation structure at the level of networks is shaped by the interplay between such local and global effects.

Analytical approximations of the correlation between the outputs of two current- or conductance-based LIF neurons in the diffusive limit have been obtained previously (de la Rocha et al., 2007; Shea-Brown et al., 2008; Tchumatchenko et al., 2008; Ostojić et al., 2009). Since integrate-and-fire models are only caricatures of actual neurons, it is useful to complement such analytical approaches with a mechanistic understanding. We characterized the mechanisms that shape correlation transfer in an intuitive way, providing insights into how correlations are affected by various aspects of neural dynamics. Moreover, the use of point processes to model inputs allowed us to address questions that are more difficult to formulate for diffusive models and helped maintain a more direct connection to physiology.

9.1 Nonstationary Inputs. Throughout this letter, we have assumed that inputs are stationary. Although this assumption is frequently made in theoretical studies (Moreno-Bote & Parga, 2006; de la Rocha et al., 2007; Shea-Brown et al., 2008; Ostojić et al., 2009), neurons in vivo receive inputs with time-dependent statistics. The assumption of stationarity is a good approximation when the input statistics change more slowly than the timescale of correlations and synaptic responses.

The dLIF model can be extended to take time-dependent rates and correlations into account while maintaining its numerical tractability. The master equation for the membrane potentials is transformed from a linear autonomous system of ODEs (see appendix D) to a linear nonautonomous system, $p'(t) = A(t)p(t)$, where $A(t)$ is the time-dependent infinitesimal generator matrix (Karlin & Taylor, 1975; Gardiner, 1985). The methods in appendix D can then be extended to investigate spiking statistics.

9.2 Alternate Measures of Correlation. There is no unique way to quantify dependencies between pairs of spike trains. We chose to use the Pearson correlation coefficient because it is a unitless quantity that is widely used and understood. However, the random walk models we presented are mathematically tractable, and our analysis can be applied to other measures of statistical dependence.

For example, measures of correlation where the covariance is normalized by the firing rates have been proposed and may offer information-theoretic advantages (Amari, 2009; Roudi, Nirenberg, & Latham, 2009). As an example, we consider the unitless convariation factor, $C_{\text{out}} = \gamma_{\text{out}}/r_{\text{out}}$. This

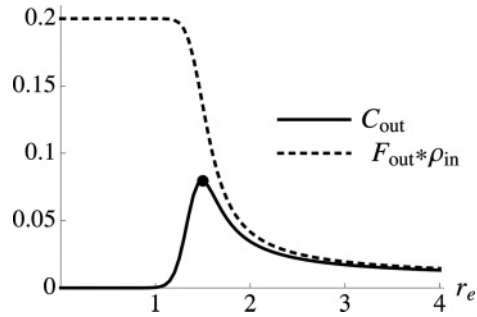

Figure 17: An alternate measure of correlation. The covariation factor (solid line) and $F_{out}\rho_{in}$ (dashed line) as a function of r_e for the dLIF with $r_i = 1$, $\bar{I}_L = 0.5$, $\rho_{ee} = \rho_{ii} = 0.2$, and $\rho_{ei} = 0$. The filled circle indicates the boundary between the drift- and fluctuation-dominated regimes, $r_e = r_i + \bar{I}_L$. The covariation factor is nearly zero for small values of r_e. As r_e grows, the cells become less forgetful and C_{out} increases initially. In the drift-dominated regime, C_{out} decreases toward $F_{out}\,\rho_{in}$ since $\rho_{out} \nearrow \rho_{in}$ (see section 3) and $\rho_{out} = C_{out}/F_{out}$.

quantity is an extension of the Fano factor that measures the dispersion of a bivariate distribution.

To analyze the covariation factor, reorganize equation 2.4 as

$$F_{out} = \mathrm{CV}^2_{out}, \text{ and } C_{out} = (F_{out} + 1)\left(\frac{E[\tau_1] - E[\tau_1 \mid V_2 \nearrow \theta]}{E[\tau_1]}\right) + S_{out}.$$

The behavior of C_{out} now parallels that of ρ_{out}. In the fluctuation-dominated limit, when $r_e \ll r_i + \bar{I}_L$, the effect of a spike in one neuron is forgotten by the time the second spikes, so that $C_{out} \approx 0$. As r_e increases toward the drift-dominated regime, the cells become less "forgetful," and $|C_{out}|$ increases. As r_e increases into the drift-dominated regime, the cells behave like PIFs, transferring spike counts linearly and preserving correlations so that $C_{out} = \rho_{out}F_{out} \approx \rho_{in}F_{out}$ (see Figure 17B).

The "forgetfulness" of cells diminishes the dependence between the output of the cells in the fluctuation-dominated regime. The effect of a spike in one neuron is forgotten before the second neuron spikes, and the output spike trains are nearly independent as a result. This is a fundamental property of excitable systems, and not due to the particular choice of the Pearson correlation coefficient or the neuron model employed.

9.3 Higher-Order Correlations. Pairwise correlations play a significant role in the neural code, and it has been proposed that the first- and second-order statistics may fully characterize the response of a population (Schneidman, Berry, Segev, & Bialek, 2006; Shlens et al., 2006, 2009; Tang et al.,

2008, although see Roudi et al., 2009). However, the higher-order structure of the population response can have significant effects on the firing of downstream neurons (Kuhn, Aertsen, & Rotter, 2003) and the information carried by the response (Roudi et al., 2009).

Equation 3.1 can be used to show that a pair of PIFs preserves higher-order correlations, and we therefore expect that a pair of leaky neurons in the drift-dominated regime approximately preserves higher-order correlations. In the fluctuation-dominated limit, the forgetfulness of cells causes spiking to become independent, and therefore higher-order correlations are reduced. The analysis of synaptic noise and coupling can also be extended to higher-order moments.

9.4 Physiologically Realistic Models. We used random walk models in our analysis and verified our results with simulations of a conductance-based integrate-and-fire model. This approach is common in studies of stochastic response properties of neurons (Salinas & Sejnowski, 2000; Rauch et al., 2003) and captures the fundamental mechanisms of a physiological cell. However, more detailed models of active conductances, synaptic plasticity, channel dynamics, and an extended dendritic morphology might reveal additional mechanisms that modulate correlations. Such models are outside the scope of this study but warrant further investigation. For instance, preliminary results suggest that correlations are reduced significantly in a Hodgkin-Huxley model (E. Shea-Brown, private communication, 2010).

Appendix A: Generating Correlated Inputs

To generate a pair of correlated Poisson processes, we used an algorithm equivalent to the SIP model in Kuhn et al. (2003). We first generated three independent Poisson processes, a_1, a_2, and b, and then defined $p_1 = a_1 + b$ and $p_2 = a_2 + b$. The processes p_1 and p_2 are correlated Poisson processes with $r_{p_j} = r_{a_j} + r_b$ and $\rho_{p_1 p_2} = r_b / \sqrt{r_{a_1} r_{a_2}}$. The cross-covariance function between these processes is a delta function with area $\gamma_{p_1 p_2} = \rho_{p_1 p_2} \sqrt{r_{p_1} r_{p_2}}$. Any pair of Poisson processes with a delta function cross-covariance is statistically equivalent to processes generated by the algorithm above. This algorithm is easily generalized to four Poisson processes with specified pairwise correlations. In generating such quadruplets, we constrain the processes so that the probability of more than two spikes occurring simultaneously is zero as $dt \to 0$. This algorithm generates delta-correlated Poisson processes. To generate pairs of Poisson processes with temporally extended correlations (for the gray lines in Figure 11), we added an independent random number to each spike time in one of the excitatory and one of the inhibitory trains. The resulting processes are Poisson with a cross-covariance function given by the density of the random numbers used (Cox & Isham, 1980).

The simulations in Figures 8 and 15 required correlated processes with CV $\neq 1$. For these simulations, we generated pairs of correlated renewal processes with gamma-distributed interspike intervals. Begin with a pair of delta-correlated Poisson processes, p_1 and p_2, generated using the algorithm above. Let $n_j \in \mathbb{N}$ be positive integers, and let g_j be the spike train consisting of every n_jth spike in p_j for $j = 1, 2$. Then g_j is a renewal processes with rate $r_{g_j} = r_{p_j}/n_j$, Fano factor $\mathrm{CV}^2 = F_{g_j} = 1/n_j$, and correlation coefficient $\rho_{g_1 g_2} = \rho_{p_1 p_2}$. The interspike intervals follow a gamma distribution with rate parameter r_{g_j} and shape parameter n_j. While the autocorrelations of such processes are oscillatory, the cross-covariance function between g_1 and g_2, is a delta function.

Appendix B: Correlation Transfer for the PIF Model

We next derive the total output correlation for a pair of PIFs driven by correlated stationary inputs. In the main text, we assume that the input signals can be written as $\mathrm{in}_j(t) = \mathrm{e}_j(t) - \mathrm{i}_j(t)$, where $\mathrm{e}_j(t)$ and $\mathrm{i}_j(t)$ are point processes. Here we derive the output statistics for a pair of PIFs driven by general stationary processes, $\mathrm{in}_1(t)$ and $\mathrm{in}_2(t)$, under weak assumptions.

We generalize the input spike count by defining $N_{\mathrm{in}_j}(t) = \int_0^t \mathrm{in}_j(s)\, ds$ for $j = 1, 2$. Note that $N_{\mathrm{in}_j}(t)$ is not necessarily integer valued since $\mathrm{in}_j(t)$ is not necessarily a point process. For the PIFs to have nonzero firing rates, we must assume that the inputs have positive mean, $\mu_{\mathrm{in}_j} = \mathrm{E}[\mathrm{in}_j(t)] > 0$. The asymptotic variances, covariance, and correlation are defined as $\sigma_{\mathrm{in}_j}(t) = \lim_{t\to\infty} \mathrm{var}(N_{\mathrm{in}_j}(t))/t$, $\gamma_{\mathrm{in}} = \lim_{t\to\infty} \mathrm{cov}(N_{\mathrm{in}_1}(t), N_{\mathrm{in}_2}(t))/t$, and $\rho_{\mathrm{in}} = \gamma_{\mathrm{in}}/(\sigma_{\mathrm{in}_1}\sigma_{\mathrm{in}_2})$. These quantities can also be interpreted in terms of the areas of auto- and cross-covariance functions as in section 2. The membrane potentials $V_1(t)$ and $V_2(t)$ of two PIFs driven by input signals $\mathrm{in}_1(t)$ and $\mathrm{in}_2(t)$ obey the stochastic equations,

$$dV_1 = \mathrm{in}_1(t)\, dt$$
$$dV_2 = \mathrm{in}_2(t)\, dt,$$

with the added condition that when V_j reaches θ_j, it is reset to $V_j = 0$ and an output spike is produced. These stochastic equations can be interpreted unambiguously in the Itô sense whenever $(N_{\mathrm{in}_1}(t), N_{\mathrm{in}_2}(t))$ is a bivariate semimartingale (Métivier, 1982). However, any interpretation that yields equation B.1 is sufficient. The output spike trains have rate, variance, covariance, and correlation r_{out_j}, $\sigma^2_{\mathrm{out}_j}$, γ_{out}, and ρ_{out} as defined in section 2. We make the following ergodicity assumptions:

1. σ_{in}, γ_{in}, σ_{out_j}, and γ_{out} are finite and $\sigma_{\mathrm{in}_j}, \sigma_{\mathrm{out}_j} > 0$
2. $\vec{V}(t) = (V_1(t), V_2(t))$ is ergodic, and its stationary distribution has finite, positive variances.

These assumptions are necessary for the outputs to be stationary and for the asymptotic input and output correlations to exist. They are true for typical processes used to model stochastic inputs, but can be violated for periodic processes or processes obtained from deterministically periodic driving forces. We assume that $\vec{V}(0)$ is drawn from the stationary distribution of $\vec{V}(t)$ so that the process is stationary. We first derive the output statistics for a pair of uncoupled PIFs driven by stationary inputs, then separately consider the case of variable synaptic responses and reciprocal coupling in appendix E.

The output spike counts are given by

$$N_{\text{out}_1}(t) = \frac{\text{in}_1(t)+V_1(0)-V_1(t)}{\theta}, \quad \text{and} \quad N_{\text{out}_2}(t) = \frac{\text{in}_2(t)+V_2(0)-V_2(t)}{\theta}. \tag{B.1}$$

Before deriving the output spiking statistics, we must prove a simple lemma. The notation $f(t) \sim o(t)$ below is shorthand for $\lim_{t\to\infty} f(t)/t = 0$:

Lemma 1. *Suppose X_t and C_t are stochastic processes such that $\lim_{t\to\infty} \text{var}(X_t)/t = c$ for some finite positive number c and $\text{var}(C_t) \sim o(t)$. Then $\text{cov}(X_t, C_t) \sim o(t)$.*

Proof. By the Cauchy-Schwarz inequality,

$$\begin{aligned}\lim_{t\to\infty} \frac{|\text{cov}(X_t, C_t)|}{t} &\le \lim_{t\to\infty} \frac{\sqrt{\text{var}(X_t)\text{var}(C_t)}}{t} = \lim_{t\to\infty} \sqrt{\frac{\text{var}(X_t)}{t}}\sqrt{\frac{\text{var}(C_t)}{t}} \\ &= 0.\end{aligned}$$

We now derive the output spiking statistics:

Theorem 1. *Under assumptions 1 and 2 above, the output spike count variance and covariance for a pair of PIFs driven by correlated stationary inputs, $in_1(t)$ and $in_2(t)$, are given by*

$$\sigma^2_{out_j} = \frac{\sigma_{in_j}}{\theta_j^2}, \quad \textit{and} \quad \gamma_{out} = \frac{\gamma_{in}}{\theta_1\theta_2}.$$

Thus, the input correlation coefficient is preserved: $\rho_{out} = \rho_{in}$.

Proof. First note that $\text{var}(V_j(t)) \sim o(t)$ by assumption 2 above and that $\lim_{t\to\infty} \text{var}(N_{\text{in}_j}(t))/t = \sigma^2_{\text{in}_j}$ is finite and positive by assumption 1. From

equation B.1 and using the bilinearity of covariances, we can calculate

$$\begin{aligned}\gamma_{\text{out}} &= \lim_{t\to\infty} \frac{1}{t}\text{cov}\left(N_{\text{out}_1}(t),\, N_{\text{out}_2}(t)\right)\\ &= \lim_{t\to\infty} \frac{1}{t}\text{cov}\left(\frac{N_{\text{in}_1}(t)+V_1(0)-V_1(t)}{\theta_1},\, \frac{N_{\text{in}_2}(t)+V_2(0)-V_2(t)}{\theta_2}\right) \quad \text{(B.2)}\\ &= \frac{1}{\theta_1\theta_2}\lim_{t\to\infty}\frac{1}{t}\left[\text{cov}\left(N_{\text{in}_1}(t),\, N_{\text{in}_2}(t)\right)+o(t)\right]\\ &= \frac{\gamma_{\text{in}}}{\theta_1\theta_2},\end{aligned}$$

where equation B.2 follows from lemma 1 and the bilinearity of covariances. Using an identical argument, we can derive $\sigma^2_{\text{out}_j} = \frac{\sigma^2_{\text{in}_j}}{\theta_j^2}$. It follows that $\rho_{\text{out}} = \gamma_{\text{out}}/(\sigma_{\text{out}_1}\sigma_{\text{out}_2}) = \rho_{\text{in}}$.

Appendix C: Derivation of Equation 2.4

In this section, we derive equation 2.4, which gives the asymptotic correlation between the outputs of two integrate-and-fire neurons. The equation holds for any integrate-and-fire models for which the membrane potentials are Markov processes (marginally and jointly) and, in addition, satisfy

$$\Pr(V_j(t_3)\in A \mid V_j(t_2)=v_2,\quad V_i(t_1)=v_1) = \Pr(V_j(t_3)\in A \mid V_j(t_2)=v_2) \quad \text{(C.1)}$$

for $i, j \in \{1, 2\}$, any set A, and any voltages v_1 and v_2 whenever $t_1 < t_2 < t_3$.

These conditions are met by a pair integrate-and-fire neurons whose subthreshold membrane potentials are governed by equations of the form

$$\begin{aligned} dV_1 &= f_1(V_1, \text{in}_1)\,dt\\ dV_2 &= f_2(V_2, \text{in}_2)\,dt,\end{aligned}$$

where $\text{in}_1(t)$ and $\text{in}_2(t)$ are stationary stochastic processes such that $\text{in}_i(t)$ is independent of $\text{in}_j(s)$ for $s \neq t$ and $i, j \in \{1, 2\}$. Here, we assume standard threshold and reset conditions at θ_j and 0, respectively (see section 2). In short, the two input processes must be delta correlated (e.g., correlated Poisson processes, white noise, or any linear combination thereof), and the neurons must be uncoupled. For example, the conditions are met for the PIF, LIF, and dLIF models considered in the text with Poisson or white noise inputs, even in the case of random synaptic amplitudes. The conditions are not strictly met for the conductance-based model due to its noninstantaneous synapses. However, the results obtained here are approximately

valid when the input is correlated in time or when synapses are not instantaneous, as long as the firing rates are significantly slower than both the synaptic time constants and the correlation time constants of the inputs.

Since the membrane potentials are marginally Markov, the output spike trains $a_1(t)$ and $a_2(t)$ are renewal processes. We assume that the bivariate membrane potential process $(V_1(t), V_2(t))$ is ergodic and its initial condition is drawn from its stationary distribution so that the output spike trains are stationary in a bivariate sense (Cox & Lewis, 1972). For ease of notation, we write $N_j(t)$ in place of $N_{a_j}(t)$ for the counting processes and similarly for other quantities.

For $t > 0$, define $Q_{ij}(t)$ to be the distribution of the waiting time until the first spike in $a_i(t)$ after a spike in $a_j(t)$:

$$Q_{ij}(t) = \lim_{\delta \to 0} \Pr(a_i \text{ spikes in } [t, t+\delta], \text{ but not in } [0,\ t] \mid a_j \text{ spikes in } [0, \delta])/\delta.$$

The auto- and cross-covariance functions are related to the asymptotic spike count statistics by (Cox & Lewis, 1972),

$$\sigma_j^2 = 2 \int_{0^+}^{\infty} R_{jj}(t)\, dt + r_j, \quad j = 1, 2$$

and

$$\gamma_{12} = \int_{0^+}^{\infty} R_{12}(t)\, dt + \int_{0^+}^{\infty} R_{21}(t)\, dt + r_s, \tag{C.2}$$

where the $+$ on the lower limit of the integrals indicates that any delta function at the origin is omitted and r_s is the rate of synchronous spikes, which accounts for the area of the omitted delta function at the origin. Similarly, r_j accounts for the area of the delta function in $R_{jj}(t)$.

Due to the renewal properties of the outputs, we have that (Cox, 1962)

$$\begin{aligned} H_{jj}(t) &:= \lim_{\delta \to 0} \frac{1}{\delta} \sum_{k=1}^{\infty} \Pr(a_j \text{ spikes for the } k\text{th time in } [t, t+\delta] \mid a_j \text{ spiked in } [0, \delta]) \\ &= \sum_{k=1}^{\infty} Q_{jj}^{(k)}(t), \quad t > 0,\ j = 1, 2, \end{aligned}$$

where $Q_{jj}^{(k)}$ is the k-fold convolution of Q_{jj} with itself. Similarly, due to the renewal properties of the outputs in addition to assumption C.1, we have

for $t > 0$,

$$\begin{aligned} H_{12}(t) &:= \lim_{\delta \to 0} \frac{1}{\delta} \sum_{k=1}^{\infty} \Pr(a_1 \text{ spikes for the } k\text{th time in} [t, t+\delta] \mid a_2 \\ &\qquad \text{spiked in } [0, \delta]) \\ &= Q_{12}(t) + \sum_{k=1}^{\infty} \left(Q_{12} * Q_{11}^{(k)} \right)(t) \\ &= Q_{12}(t) + (Q_{12} * H_{11})(t), \end{aligned} \tag{C.3}$$

where $*$ denotes convolution. Similarly, $H_{21}(t) = Q_{21}(t) + (Q_{21} * H_{22})(t)$ for $t > 0$.

We proceed by considering the Laplace transform of the cross-covariance functions. The Laplace transform of a function $f(t)$ is given by $\hat{f}(u) = \int_{0^+}^{\infty} e^{-ut} f(t)\, dt$. Using elementary properties of the Laplace transform, equation C.3 can be rewritten as $\hat{H}_{12}(u) = \hat{Q}_{12}(u) + \hat{Q}_{12}(u)\hat{H}_{11}(u)$. Now, using the definition of $R_{12}(t)$, we can write

$$\begin{aligned} \hat{R}_{12}(u) &= r_2 \left(\hat{H}_{12}(u) - \frac{r_1}{u} \right) \\ &= r_2 \left(\hat{Q}_{12}(u) + \hat{Q}_{12}(u)\hat{H}_{11}(u) - \frac{r_1}{u} \right) \\ &= r_2 \left(\hat{Q}_{12}(u) + \frac{1}{r_1} \hat{Q}_{12}(u)\hat{R}_{11}(u) + r_1 \left(\frac{\hat{Q}_{12}(u) - 1}{u} \right) \right), \end{aligned}$$

where the last step follows from the fact that $\hat{H}_{11}(u) = \hat{R}_{11}(u)/r_1 + r_1/u$. From this, we can calculate the area of the cross-covariance function,

$$\begin{aligned} \int_{0^+}^{\infty} R_{12}(t)\, dt &= \lim_{u \to 0} \hat{R}_{12}(u) \\ &= r_2 \left(1 + \frac{\sigma_1^2 - r_1}{2r_1} + r_1 \hat{Q}'_{12}(0) \right) \\ &= r_2 \left(\frac{\mathrm{CV}_1^2 + 1}{2} - r_1 E[\tau_1 \mid V_2 \nearrow \theta_2] \right) \end{aligned} \tag{C.4}$$

where $F_1 = \mathrm{CV}_1^2 = \sigma_1^2 / r_1$ is the output Fano factor and $E[\tau_1 \mid V_2 \nearrow \theta_2] = -\hat{Q}'_{12}(0)$ is the expected time until the first spike in a_1 after a spike in a_2 (Feller, 1991). In the derivation above, we used the facts that $\lim_{u \to 0} \hat{Q}_{12}(u) = 1$ and $\lim_{u \to 0} \hat{R}_{11}(u) = (\sigma_1^2 - r_1)/2$.

By an identical argument, we get an analogous expression for $\int_{0^+}^{\infty} R_{21}(t)\,dt$. From these expressions and equation C.2, we can write the output correlation, $\rho_{\text{out}} = \gamma_{12}/(\sigma_1\sigma_2)$, as

$$\rho_{\text{out}} = \frac{\sqrt{r_1 r_2}\,(E[\tau_1] - E[\tau_1 \mid V_2 \nearrow \theta_2] + E[\tau_2] - E[\tau_2 \mid V_1 \nearrow \theta_1]) + S_{12}}{\text{CV}_1\text{CV}_2}, \tag{C.5}$$

where $E[\tau_1] = (\text{CV}_1^2 + 1)/(2r_1)$ is the expected recurrence time (Cox, 1962), which is the expected time until the next spike in a_1 starting from an arbitrary time (i.e., with V_1 starting from its stationary distribution) and similarly for $E[\tau_2]$.

To obtain the form given in equation 2.4, we note that equation C.4 can be written as

$$\int_{0^+}^{\infty} R_{12}(t)\,dt = \frac{r_2}{2}(\text{CV}_1^2 + 1)\left(\frac{E[\tau_1] - E[\tau_1 \mid V_2 \nearrow \theta_2]}{E[\tau_1]}\right).$$

In the symmetric case, combining this with equation C.2 gives equation 2.4.

Equation C.5 can be used to calculate the correlation between simulated data when the model satisfies the Markov assumptions made above. To apply the equation to data, we need only to obtain estimates for r_j, CV_j, $E[\tau_1 \mid V_2 \nearrow \theta_2]$, $E[\tau_2 \mid V_1 \nearrow \theta_1]$, and S_{12}. The rates and ISI CVs can easily be estimated from a sample of the univariate interspike intervals, $r_j = 1/E[I\,Si_j]$ and $\text{CV}_j^2 = \text{var}(I\,Si_j)/E[I\,Si_j]^2$. The synchrony is easily estimated by counting the occurrence of synchronous spikes. To estimate $E[\tau_1 \mid V_2 \nearrow \theta_2]$, one needs only to calculate the average time between a spike in a_2 and the next spike in a_1, and similarly for $E[\tau_2 \mid V_1 \nearrow \theta_1]$.

We used equation C.5 to obtain the estimates of ρ_{out} for the LIF model in Figures 4 and 8. We found several advantages to using this method versus conventional methods, such as computing the cross-covariance functions or counting spikes over sliding windows. When calculating the correlation from the integrals of the cross-covariance functions, one must bin time and also choose a large window size over which to integrate. Similarly, when using the sample covariance of spike counts between sliding windows, one must choose a large window size for the sliding window. The quantities in equation C.5 can all be estimated by looking at the time intervals between spikes. It is therefore not necessary to bin time or fix a large window size over which to calculate the correlation. The algorithm based on equation C.5 appears to be faster than algorithms using the other two methods. Although a deeper investigation is necessary, it also appears that the estimator is more accurate.

Next, we show how equation C.5 can be used to calculate the exact correlation coefficient for the dLIF model.

Appendix D: Analysis of the dLIF Model

The methods used to analyze the PIF model cannot be applied to the dLIF model since there is no analog to equation 3.1 due to the lower reflecting barrier at β. However, when the inputs are correlated Poisson processes as defined in appendix A, we can use the theory of continuous-time Markov chains in combination with equation C.5 to derive the output spiking statistics. (A suite of Matlab programs that implement the methods described below can be found online at http://www.mathworks.com/matlabcentral/fileexchange/28686.)

For notational simplicity in the analysis below, we consider only the case where $\bar{I}_L = 0$, that is, there is no leak term. However, note that the leak current in this model is equivalent to an uncorrelated inhibitory input current. To recover the results for $\bar{I}_L > 0$ from the results below, simply make the substitutions $r_{\mathrm{i}_j} \to r_{\mathrm{i}_j} + \bar{I}_{L_j}$, $\rho_{\mathrm{ii}} \to \rho_{\mathrm{ii}}/(1 + \bar{I}_L/r_{\mathrm{i}})$, and $\rho_{\mathrm{ei}} \to \rho_{\mathrm{ei}}/\sqrt{1 + \bar{I}_L/r_{\mathrm{i}}}$.

We first derive the univariate statistics for a single dLIF driven by Poisson inputs (see section 2). The membrane potential $V(t)$ for this model is a continuous-time Markov random walk, and the output spike trains are renewal processes. The Laplace transform of the first passage time densities for reflected random walks are obtained by Khantha and Balakrishnan (1983). The moments of the first passage times can be found from the derivatives of these Laplace transforms (Feller, 1991). For the mean first passage time of $V(t)$ over θ starting from $k \in \{\beta, \beta + 1, \ldots, \theta - 1\}$,

$$\mu_{k\to\theta} = \frac{q\left(-q^{\beta-k} - kq + k + q^{\beta-\theta} + q\theta - \theta\right)}{(q-1)^2 r_{\mathrm{e}}}.$$

To derive this expression, we needed to correct an error in Khantha and Balakrishnan (1983) in going from their equation 6 to equation 7: the inner expression in their equation 7 should read $(m - m_0) + (f^{-m} - f^{-m_0})/(f - 1)$ instead of $(m - m_0) - (f^{-m} - f^{-m_0})/(f - 1)$. The variance of the first passage time from reset to threshold is given by

$$\sigma^2_{0\to\theta} = \frac{q^2\left(-4(\beta(q-1) - q(\theta+1) + \theta)q^{\beta-\theta} + q^{2(\beta-\theta)} - q^{2\beta} + 4(\beta(q-1) - q)q^{\beta} + \left(q^2-1\right)\theta\right)}{(q-1)^4 r_{\mathrm{e}}^2}.$$

The output firing rate is then given by $r_{\mathrm{out}} = 1/\mu_{0\to\theta}$, the asymptotic spike count variance is $\sigma^2_{\mathrm{out}} = \sigma^2_{0\to\theta}/\mu^3_{0\to\theta}$, and the output Fano factor is $F_{\mathrm{out}} = \mathrm{CV}^2_{\mathrm{out}} = \sigma^2_{0\to\theta}/\mu^2_{0\to\theta} = \sigma^2_{\mathrm{out}}/r_{\mathrm{out}}$ (Cox, 1962). Simplified expressions for r_{out} and $\mathrm{CV}_{\mathrm{out}}$ are given in section 2.

Other univariate statistics can be found from the infinitesimal generator matrix of the membrane potential process, $V(t)$ (Karlin & Taylor, 1975). The off-diagonal terms ($i \neq j$) of this matrix are given by

$$\mathcal{B}_{ij} := \lim_{h\to 0} \frac{1}{h}\Pr(V(t+h) = j \mid V(t) = i) = \begin{cases} r_{\mathrm{e}} & j = i+1 \\ r_{\mathrm{i}} & j = i-1 \\ r_{\mathrm{e}} & i = \theta - 1,\ j = 0 \end{cases}. \quad \text{(D.1)}$$

The diagonal terms are then chosen so that each row sums to zero: $\mathcal{B}_{ii} = -\sum_{j \neq i} \mathcal{B}_{ij}$. The distribution of $V(t)$ is then given by $P(t) = P(0)e^{\mathcal{B}t}$, where $P(t)$ is a time-dependent vector with $P_j(t) = \Pr(V(t) = j)$ and $P(0)$ is the initial distribution. The stationary distribution $p(j) = \lim_{t\to\infty} P_j(t)$ is then given by the left eigenvector corresponding to the dominant left eigenvalue, $\lambda_0 = 0$. The remaining eigenvalues have negative real part. The nonzero eigenvalue with maximal real part, λ_1, determines the timescale with which $P_j(t) \to p(j)$. In particular, $|P_j(t) - p(j)| \sim e^{-t/\tau_{\text{mem}}}$, where $\tau_{\text{mem}} = -1/\text{Real}(\lambda_1)$.

The univariate stationary distribution, $p(j)$, can be found by deriving the dominant left eigenvector as discussed above, which is equivalent to solving the detailed balance equation $p = pe^{\mathcal{B}}$. This is a linear recurrence equation and can be solved using a computer algebra system or by hand using the method of generating functions. We obtained the solution

$$p(k) = \lim_{t\to\infty} \Pr(V(t) = k) = \frac{q-1}{q^\beta - q^\theta(q^\beta + \theta - q\theta)} \times \begin{cases} (q^{\theta+k} - q^k) & \beta \le k \le 0 \\ (q^\theta - q^k) & 0 < k < \theta \end{cases}. \tag{D.2}$$

The output rate, derived from the first passage properties above is also given by the probability flux across threshold: $r_{\text{out}} = r_e p(\theta - 1)$.

We now consider the case of two dLIF neurons driven by correlated Poisson inputs (see section 2). We will use equation C.5 to calculate the correlation coefficient, ρ_{out}, between the output spike trains. First, we must calculate the stationary distribution of the bivariate process, $(V_1(t), V_2(t))$. We first enumerate the state-space, $\theta_1 \times \theta_2$ into a single vector of length $\theta_1\theta_2$ and calculate the infinitesimal generator matrix, in a similar fashion to the univariate case described above. Complicated boundary conditions make it impractical to include the full bivariate generator matrix in the text. The Matlab code that accompanies this letter can be used to generate this matrix.

The bivariate stationary distribution, $p(k_1, k_2)$, is the the basis vector for the one-dimensional nullspace of the transpose of $\mathcal{A}$; equivalently, it is the left eigenvector of $\mathcal{A}$ associated with the left eigenvalue $\lambda = 0$. A variety of numerical techniques can be used for finding this vector. Note that the vector must be normalized so that its elements sum to 1 since $p(k_1, k_2)$ is a probability distribution.

A synchronous output spike occurs whenever both cells are just below threshold and receive a synchronous excitatory input. The rate of synchronous outputs spike is therefore given by $r_s = p(\theta_1 - 1, \theta_2 - 1)\rho_{\text{ee}}\sqrt{r_{\text{e}_1} r_{\text{e}_2}}$. The output synchrony is then $S_{12} = r_s/\sqrt{r_{\text{out}_1} r_{\text{out}_2}}$.

Since the univariate statistics are known in closed form (see above), the only quantities from equation C.5 left to calculate are $E[\tau_1 \mid V_2 \nearrow \theta_2]$ and

$E[\tau_2 \mid V_1 \nearrow \theta_1]$. First, define the conditional distribution,

$$p_1(k_1 \mid V_2 = \theta_2 - 1) = \frac{p(k_1, \theta_2 - 1)}{p_2(\theta_2 - 1)},$$

where $p_2(\theta_2 - 1)$ is the value of univariate stationary distribution for $V_2(t)$ at $\theta_2 - 1$ from equation D.2. From here, we need to calculate the conditional distribution $p_1(k_1 \mid V_2 \nearrow \theta_2)$, which represents the distribution of V_1 given that V_2 has just crossed threshold. This can be calculated by evolving a proportion $\rho_{\mathrm{ee}}\sqrt{r_{\mathrm{e}_1}/r_{\mathrm{e}_2}}$ of the probability mass in $p(k_1 \mid V_2 = \theta_2 - 1)$ by one excitatory spike and evolving a separate proportion $\rho_{\mathrm{i}_1\mathrm{e}_2}\sqrt{r_{\mathrm{i}_1}/r_{\mathrm{e}_2}}$ by one inhibitory spike (see the linked Matlab code). We can then use the mean first passage times derived above to calculate

$$E[\tau_1 \mid V_2 \nearrow \theta_2] = \sum_{k=\beta_1}^{\theta_1} p(k \mid V_2 \nearrow \theta_2)\, \mu_{k \to \theta_1}.$$

An identical method is used to calculate $E[\tau_2 \mid V_1 \nearrow \theta_1]$. Now, ρ_{out} can be calculated from equation C.5.

We now describe how to calculate time-dependent statistics for Figures 5 and 17A. Let $\mathcal{B}_1$ be the infinitesimal generator matrix of the marginal process $V_1(t)$ (see equation D.1). Given an initial distribution, $V_1(0)$, the distribution of $V_1(t)$ is given by $e^{\mathcal{B}_1 t}V_1(0)$. The conditional distribution of $V_1(t)$ after a spike in V_2 is then given by $\Pr(V_1(t) = k \mid V_2(0) \nearrow \theta_2) = \left[e^{\mathcal{B}_1 t}V_1(0)\right]_k$, where $[\cdot]_k$ denotes the kth component and the initial distribution is the conditional distribution described above, $[V_1(0)]_k = p_1(k \mid V_2 \nearrow \theta_2)$.

The time-dependent conditional mean and standard deviation for the top row of Figure 5 can be calculated directly from $p_1(k_1 \mid V_2 \nearrow \theta_2)$. The instantaneous firing rate, given an initial distribution $V_1(0)$, is given by the flux across threshold, $\nu(t \mid V_1(0)) = r_{\mathrm{e}}\left[e^{\mathcal{B}_1 t}V_1(0)\right]_{\theta_1 - 1}$. The conditional intensity function, $H_{12}(t)$, is then given by $\nu(t \mid V_1(0))$ with $[V_1(0)]_k = p_1(k \mid V_2 \nearrow \theta_2)$. The autoconditional intensity function, $H_{11}(t)$, is given by $\nu(t \mid V_1(0))$ with $[V_1(0)]_k = \delta_{0,k}$. The functions $H_{21}(t)$ and $H_{22}(t)$ are derived analogously. The auto- and cross-covariance functions are then given by $R_{ij}(t) = r_j(H_{ij}(t) - r_{\mathrm{i}})$.

For the bottom row of Figure 5, we needed to calculate the cumulative distribution of the first passage time of V_1 over θ_1 given an initial distribution. This can be achieved by adding an absorbing state at threshold, θ_2, to the marginal infinitesimal generator, $\mathcal{B}_1$. Then the cumulative distribution of the waiting time until the next spike is simply given by the amount of mass in the absorbing state at time t. That is, $\Pr(\tau_1 \le t) = \left[e^{\mathcal{B}_1 t}V_1(0)\right]_{\theta_1}$, where $\mathcal{B}_1$ has an absorbing state at θ_1, and $V_1(0)$ is the appropriate initial distribution. The conditional distribution (the solid line in the bottom row

of Figure 5) is found by setting $[V_1(0)]_k = p_1(k \mid V_2 \nearrow \theta_2)$ as above. The stationary case (dashed line) is found by setting $[V_1(0)]_k = p_1(k)$, where $p_1(k)$ is the marginal stationary distribution from equation D.2.

Appendix E: Generalizations of the PIF Model

In this section, we generalize theorem 1 to take synaptic variability and coupling into account in the PIF model, thereby obtaining the main equations in sections 5 and 6.

E.1 The PIF with Random Postsynaptic Responses. Suppose that the ith excitatory input to neuron j increments $V_j(t)$ by a random amount $d^i_{\mathrm{e}_j}$ and that the ith inhibitory input to neuron j decrements $V_j(t)$ by a random amount $d^i_{\mathrm{i}_j}$. Each $d^i_{\mathrm{e}_j}$ ($d^i_{\mathrm{i}_j}$) is drawn independently from a distribution with mean $\overline{d}_{\mathrm{e}_j}$ ($\overline{d}_{\mathrm{i}_j}$) and variance $\sigma^2_{d_{\mathrm{e}_j}}$ ($\sigma^2_{d_{\mathrm{i}_j}}$) for $j = 1, 2$. To guarantee positive firing rates $r_{\mathrm{out}_j} = (r_{\mathrm{e}_j}\overline{d}_{\mathrm{e}_j} - r_{\mathrm{i}_j}\overline{d}_{\mathrm{i}_j})/\theta_j > 0$, we assume $\mu_{Y_j} = r_{\mathrm{e}_j}\overline{d}_{\mathrm{e}_j} - r_{\mathrm{i}_j}\overline{d}_{\mathrm{i}_j} > 0$. This model is equivalent to a PIF with inputs

$$Y_j(t) = \sum_{t_i \in \Gamma_{\mathrm{e}_j}} d^i_{\mathrm{e}_j}\delta(t - t_i) - \sum_{t_i \in \Gamma_{\mathrm{i}_j}} d^i_{\mathrm{i}_j}\delta(t - t_i), \quad j = 1, 2.$$

Thus, by theorem 1, $\sigma^2_{\mathrm{out}_1} = \frac{\sigma^2_{Y_j}}{\theta_j^2}$, $\gamma_{\mathrm{out}} = \frac{\gamma_{Y_1Y_2}}{\theta_1\theta_2}$, and $\rho_{\mathrm{out}} = \rho_{Y_1Y_2}$.

The accumulated effective input process $N_{Y_j}(t) = \int_0^t Y_j(s)\,ds$ can be written as

$$N_{Y_j}(t) = \sum_{i=1}^{N_{\mathrm{e}_j}(t)} d^i_{\mathrm{e}_j} - \sum_{i=1}^{N_{\mathrm{i}_j}(t)} d^i_{\mathrm{i}_j}. \tag{E.1}$$

The two terms on the right-hand side of eq. E.1 are random sums with variances (Karlin & Taylor, 1975) given by

$$\mathrm{var}(N_{Y_j}(t)) = \mathrm{var}(N_{\mathrm{e}_j}(t))\overline{d}^2_{\mathrm{e}_j} + E[N_{\mathrm{e}_j}(t)]\sigma^2_{d_{\mathrm{e}_j}} + \mathrm{var}(N_{\mathrm{i}_j}(t))\overline{d}_{\mathrm{i}_j} + E[N_{\mathrm{i}_j}(t)]\sigma^2_{d_{\mathrm{i}_j}}.$$

Dividing by t and taking $t \to \infty$ gives

$$\sigma^2_{Y_j} = \lim_{t\to\infty}\frac{1}{t}\mathrm{var}(N_{Y_j}(t)) = \sigma^2_{\mathrm{e}_j}\overline{d}^2_{\mathrm{e}_j} + r_{\mathrm{e}_j}\sigma^2_{d_{\mathrm{e}_j}} + \sigma^2_{\mathrm{i}_j}\overline{d}^2_{\mathrm{i}_j} + r_{\mathrm{i}_j}\sigma^2_{d_{\mathrm{i}_j}}.$$

Covariances can be derived similarly to obtain

$$\gamma_{Y_1Y_2} = \overline{d}_{\mathrm{e}_1}\overline{d}_{\mathrm{e}_2}\gamma_{\mathrm{e}_1\mathrm{e}_2} + \overline{d}_{\mathrm{i}_1}\overline{d}_{\mathrm{i}_2}\gamma_{\mathrm{i}_1\mathrm{i}_2} - \overline{d}_{\mathrm{e}_1}\overline{d}_{\mathrm{i}_2}\gamma_{\mathrm{e}_1\mathrm{i}_2} - \overline{d}_{\mathrm{i}_1}\overline{d}_{\mathrm{e}_2}\gamma_{\mathrm{i}_1\mathrm{e}_2}.$$

Thus,

$$\sigma^2_{\mathrm{out}_j} = \left(\sigma^2_{\mathrm{e}_j}\overline{d}^2_{\mathrm{e}_j} + r_{\mathrm{e}_j}\sigma^2_{d_{\mathrm{e}_j}} + \sigma^2_{\mathrm{i}_j}\overline{d}^2_{\mathrm{i}_j} + r_{\mathrm{i}_j}\sigma^2_{d_{\mathrm{i}_j}}\right)/\theta_j^2,$$

and

$$\gamma_{\mathrm{out}} = \left(\overline{d}_{\mathrm{e}_1}\overline{d}_{\mathrm{e}_2}\gamma_{\mathrm{e}_1\mathrm{e}_2} + \overline{d}_{\mathrm{i}_1}\overline{d}_{\mathrm{i}_2}\gamma_{\mathrm{i}_1\mathrm{i}_2} - \overline{d}_{\mathrm{e}_1}\overline{d}_{\mathrm{i}_2}\gamma_{\mathrm{e}_1\mathrm{i}_2} - \overline{d}_{\mathrm{i}_1}\overline{d}_{\mathrm{e}_2}\gamma_{\mathrm{i}_1\mathrm{e}_2}\right)/\left(\theta_1\theta_2\right),$$

and therefore

$$\rho_{\mathrm{out}} = \frac{\overline{d}_{\mathrm{e}_1}\overline{d}_{\mathrm{e}_2}\gamma_{\mathrm{e}_1\mathrm{e}_2} + \overline{d}_{\mathrm{i}_1}\overline{d}_{\mathrm{i}_2}\gamma_{\mathrm{i}_1\mathrm{i}_2} - \overline{d}_{\mathrm{e}_1}\overline{d}_{\mathrm{i}_2}\gamma_{\mathrm{e}_1\mathrm{i}_2} - \overline{d}_{\mathrm{i}_1}\overline{d}_{\mathrm{e}_2}\gamma_{\mathrm{i}_1\mathrm{e}_2}}{\sqrt{\left(\sigma^2_{\mathrm{e}_1}\overline{d}^2_{\mathrm{e}_1} + r_{\mathrm{e}_1}\sigma^2_{d_{\mathrm{e}_1}} + \sigma^2_{\mathrm{i}_1}\overline{d}^2_{\mathrm{i}_1} + r_{\mathrm{i}_1}\sigma^2_{d_{\mathrm{i}_1}}\right)\left(\sigma^2_{\mathrm{e}_2}\overline{d}^2_{\mathrm{e}_2} + r_{\mathrm{e}_2}\sigma^2_{d_{\mathrm{e}_2}} + \sigma^2_{\mathrm{i}_2}\overline{d}^2_{\mathrm{i}_2} + r_{\mathrm{i}_2}\sigma^2_{d_{\mathrm{i}_2}}\right)}}.$$

In the symmetric case discussed in the text, this simplifies to equation 5.1.

To combine variable PSP amplitudes—independent and identically distributed (i.i.d.) random jumps, d_{i}, with $\mathrm{CV} = \mathrm{CV}_d$—with synaptic failure (probability of release p), we can multiply each jump d_{i} by an i.i.d. binomial variable, b_i (with $\Pr(b_i = 1) = p$), to obtain the "effective" jumps. In the symmetric case, the CV of this product is given by $\sqrt{(\mathrm{CV}_d^2 + 1 - p)/p}$. Making the substitution $\mathrm{CV}_d \to \sqrt{(\mathrm{CV}_d^2 + 1 - p)/p}$ in equation (5.1 gives equation 5.2).

E.2 The PIF with Coupling. Now suppose that the subthreshold membrane potentials $V_1(t)$ and $V_2(t)$ of the PIFs driven by the stationary signals $\mathrm{in}_1(t)$ and $\mathrm{in}_2(t)$ obey the coupled equations,

$$\begin{aligned} dV_1 &= \mathrm{in}_1(t)\,dt + c_1\mathrm{out}_2(t)\,dt \\ dV_2 &= \mathrm{in}_2(t)\,dt + c_2\mathrm{out}_1(t)\,dt, \end{aligned}$$

with out_1 and out_2 the output spike trains. Thus, each output spike from neuron 2 increments V_1 by an amount c_1, and vice versa. We assume that $c_j < \theta_j$ so that a spike from one neuron cannot drive the other from reset to threshold. Then the output spike counts obey the coupled equations,

$$\begin{aligned} N_{\mathrm{out}_1}(t) &= \frac{\mathrm{in}_1(t) + c_1 N_{\mathrm{out}_2}(t) + V_1(0) - V_1(t)}{\theta} \\ N_{\mathrm{out}_2}(t) &= \frac{\mathrm{in}_2(t) + c_2 N_{\mathrm{out}_1}(t) + V_2(0) - V_2(t)}{\theta}. \end{aligned} \tag{E.2}$$

Defining $n_j(t) = N_{\text{in}_j}(t) + V_j(0) - V_j(t)$, we can solve equation E.2 for $N_{\text{out}_j}(t)$ to obtain

$$N_{\text{out}_1}(t) = \frac{\theta_2 n_1(t) + c_1 n_2(t)}{\theta_1\theta_2 - c_1c_2}, \quad N_{\text{out}_2}(t) = \frac{\theta_1 n_2(t) + c_2 n_1(t)}{\theta_1\theta_2 - c_1c_2}. \tag{E.3}$$

Thus, in order to have nonzero firing rates, we must assume that $\theta_2\mu_{\text{in}_1} + c_1\mu_{\text{in}_2} > 0$ and $\theta_1\mu_{\text{in}_2} + c_2\mu_{\text{in}_1} > 0$ and the firing rates are $r_{\text{out}_1} = (\theta_2\mu_{\text{in}_1} + c_1\mu_{\text{in}_2})/(\theta_1\theta_2 - c_1c_2)$ and $r_{\text{out}_2} = (\theta_1\mu_{\text{in}_2} + c_2\mu_{\text{in}_1})/(\theta_1\theta_2 - c_1c_2)$.

The following theorem gives the total output correlation:

Theorem 2. *The output correlation coefficient between the output of a pair of coupled PIFs driven by correlated stationary inputs $in_1(t)$ and $in_2(t)$ with coupling terms c_1 and c_2 is*

$$\rho_{out} = \frac{(\theta_1\theta_2 + c_1c_2)\gamma_{in} + c_2\theta_2\sigma^2_{in_1} + c_1\theta_1\sigma^2_{in_2}}{\sqrt{\left(\theta_2^2\sigma^2_{in_1} + c_1^2\sigma^2_{in_2} + 2c_1\theta_2\gamma_{in}\right)\left(\theta_1^2\sigma^2_{in_2} + c_2^2\sigma^2_{in_1} + 2c_2\theta_1\gamma_{in}\right)}}. \tag{E.4}$$

Proof From equation E.3,

$$\begin{aligned}
\gamma_{\text{out}} &= \lim_{t\to\infty}\frac{1}{t}\text{cov}\left(N_{\text{out}_1}(t), N_{\text{out}_2}(t)\right) \\
&= \lim_{t\to\infty}\frac{1}{t}\text{cov}\left(\frac{\theta_2 n_1(t) + c_1 n_2(t)}{\theta_1\theta_2 - c_1c_2}, \frac{\theta_1 n_2(t) + c_2 n_1(t)}{\theta_1\theta_2 - c_1c_2}\right) \\
&= \frac{1}{(\theta_1\theta_2 - c_1c_2)^2}\lim_{t\to\infty}\frac{1}{t}\text{cov}\left(\theta_2 n_1(t) + c_1 n_2(t), \theta_1 n_2(t) + c_2 n_1(t)\right) \\
&= \frac{1}{(\theta_1\theta_2 - c_1c_2)^2}\left((\theta_1\theta_2 + c_1c_2)\gamma_{n_1n_2} + c_2\theta_2\sigma^2_{n_1} + c_1\theta_1\sigma^2_{n_2}\right).
\end{aligned}$$

By an identical argument,

$$\sigma^2_{\text{out}_1} = \frac{1}{(\theta_1\theta_2 - c_1c_2)^2}\left(\theta_2^2\sigma^2_{n_1} + c_1^2\sigma^2_{n_2} + 2c_1\theta_2\gamma_{n_1n_2}\right),$$

with a a symmetric expression for $\sigma^2_{\text{out}_2}$. Therefore,

$$\begin{aligned}
\rho_{\text{out}} &= \frac{\gamma_{\text{out}}}{\sigma_{\text{out}_1}\sigma_{\text{out}_2}} \\
&= \frac{(\theta_1\theta_2 + c_1c_2)\gamma_{n_1n_2} + c_2\theta_2\sigma^2_{n_1} + c_1\theta_1\sigma^2_{n_2}}{\sqrt{\left(\theta_2^2\sigma^2_{n_1} + c_1^2\sigma^2_{n_2} + 2c_1\theta_2\gamma_{n_1n_2}\right)\left(\theta_1^2\sigma^2_{n_2} + c_2^2\sigma^2_{n_1} + 2c_2\theta_1\gamma_{n_1n_2}\right)}}.
\end{aligned} \tag{E.5}$$

All that is left is to show that $\sigma_{n_j} = \sigma_{\text{in}_j}$ and $\gamma_{n_1 n_2} = \gamma_{\text{in}}$. We have

$$\begin{aligned}
\gamma_{n_1 n_2} &= \lim_{t\to\infty} \frac{1}{t} \text{cov}\,(n_1(t), n_2(t)) \\
&= \lim_{t\to\infty} \frac{1}{t} \text{cov}\,(N_{\text{in}_1}(t) + V_1(0) - V_1(t),\, N_{\text{in}_2}(t) + V_2(0) - V_2(t)) \\
&= \lim_{t\to\infty} \frac{1}{t} \left(\text{cov}\,(N_{\text{in}_1}(t), N_{\text{in}_2}(t)) + o(t)\right) \qquad \text{(E.6)} \\
&= \gamma_{\text{in}},
\end{aligned}$$

where equation E.6 follows from lemma 1 and the assumption that $(V_1(t), V_2(t))$ is ergodic with finite second moments. By an identical argument, we have $\sigma^2_{n_j} = \sigma^2_{\text{in}_j}, \quad j = 1, 2.$

In the symmetric case, we define $u = c/\theta$ and obtain equation 6.1.

Acknowledgments

We thank Brent Doiron, Eric Shea-Brown, Jaime de la Rocha, Nick Cain, and Cheng Ly for helpful discussions. This work was supported by NSF grants DMS-0604429 and DMS-0817649 and a Texas ARP/ATP award.

References

Allen, C., & Stevens, C. (1994). An evaluation of causes for unreliability of synaptic transmission. *Proc. Natl. Acad. Sci. USA, 91*(22), 10380–10383.

Amari, S. (2009). Measure of correlation orthogonal to change in firing rate. *Neural Comput., 21*(4), 960–972.

Averbeck, B., Latham, P., & Pouget, A. (2006). Neural correlations, population coding and computation. *Nature Rev. Neurosci., 7*(5), 358–366.

Biederlack, J., Castelo-Branco, M., Neuenschwander, S., Wheeler, D., Singer, W., & Nikolić, D. (2006). Brightness induction: Rate enhancement and neuronal synchronization as complementary codes. *Neuron, 52*(6), 1073–1083.

Brémaud, A., West, D., & Thomson, A. (2007). Binomial parameters differ across neocortical layers and with different classes of connections in adult rat and cat neocortex. *Proc. Natl. Acad. Sci. USA, 104*(35), 14134–14139.

Brody, C. (1999). Correlations without synchrony. *Neural Comput., 11*(7), 1537–1551.

Brunel, N., Chance, F., Fourcaud, N., & Abbott, L. (2001). Effects of synaptic noise and filtering on the frequency response of spiking neurons. *Phys. Rev. Lett., 86*(10), 2186–2189.

Burkitt, A. (2006). A review of the integrate-and-fire neuron model, I. Homogeneous synaptic input. *Biol. Cybern., 95*(1), 1–19.

Cohen, M., & Maunsell, J. (2009). Attention improves performance primarily by reducing interneuronal correlations. *Nat. Neurosci., 12*(12), 1594–1600.

Cox, D. (1962). *Renewal theory*. London: Methuen.

Cox, D., & Isham, V. (1980). *Point processes*. London: Chapman and Hall.
Cox, D., & Lewis, P. (1972). Multivariate point processes. In *Proc. Sixth Berkeley Symp. on Math. Stat. and Prob.* (pp. 401–448). Berkeley: University of California Press.
Czubayko, U., & Plenz, D. (2002). Fast synaptic transmission between striatal spiny projection neurons. *Proc. Natl. Acad. Sci. USA, 99*(24), 15764–15769.
Daley, D., & Vere-Jones, D. (2003). *An introduction to the theory of point processes*. New York: Springer.
Dan, Y., Alonso, J., Usrey, W., & Reid, R. (1998). Coding of visual information by precisely correlated spikes in the lateral geniculate nucleus. *Nat. Neurosci., 1*(6), 501–507.
Dayan, P., & Abbott, L. (2001). *Theoretical neuroscience: Computational and mathematical modeling of neural systems*. Cambridge, MA: MIT Press.
de la Rocha, J., Doiron, B., Shea-Brown, E., Josić, K., & Reyes, A. (2007). Correlation between neural spike trains increases with firing rate. *Nature, 448*(7155), 802–806.
Ecker, A., Berens, P., Keliris, G., Bethge, M., Logothetis, N., & Tolias, A. (2010). Decorrelated neuronal firing in cortical microcircuits. *Science, 327*(5965), 584–587.
Feller, W. (1991). *An introduction to probability theory and its applications*. Hoboken, NJ: Wiley.
Fusi, S., & Mattia, M. (1999). Collective behavior of networks with linear (VLSI) integrate-and-fire neurons. *Neural Comput., 11*(3), 633–652.
Gardiner, C. (1985). *Handbook of stochastic methods*. Berlin: Springer.
Gawne, T., & Richmond, B. (1993). How independent are the messages carried by adjacent inferior temporal cortical neurons? *J. Neurosci., 13*(7), 2758–2771.
Gerstein, G., & Mandelbrot, B. (1964). Random walk models for the spike activity of a single neuron. *Biophys. J., 4*, 41–68.
Gibson, J., Beierlein, M., & Connors, B. (1999). Two networks of electrically coupled inhibitory neurons in neocortex. *Nature, 402*(6757), 75–79.
Gutnisky, D., & Dragoi, V. (2008). Adaptive coding of visual information in neural populations. *Nature, 452*(7184), 220–224.
Helias, M., Deger, M., Rotter, S., & Diesmann, M. (2010). Instantaneous non-linear processing by pulse-coupled threshold units. *PLoS Comput. Biol., 6*(9), e1000929.
Hertz, J. (2010). Cross-correlations in high-conductance states of a model cortical network. *Neural Comp., 22*(2), 427–447.
Hessler, N., Shirke, A., & Malinow, R. (1993). The probability of transmitter release at a mammalian central synapse. *Nature, 366*, 569–572.
Josić, K., Shea-Brown, E., Doiron, B., & de la Rocha, J. (2009). Stimulus-dependent correlations and population codes. *Neural Comput., 21*(10), 2774–2804.
Karlin, S., & Taylor, H. (1975). *A first course in stochastic processes*. Orlando, FL: Academic Press.
Khantha, M., & Balakrishnan, V. (1983). First passage time distributions for finite one-dimensional random walks. *Pramana, 21*(2), 111–122.
Kisvárday, Z., Tóth, E., Rausch, M., & Eysel, U. (1997). Orientation-specific relationship between populations of excitatory and inhibitory lateral connections in the visual cortex of the cat. *Cereb. Cortex, 7*(7), 605–618.
Knight, B. (1972). Dynamics of encoding in a population of neurons. *J. Gen. Physiol., 59*(6), 734–766.

Kobayashi, R., Tsubo, Y., & Shinomoto, S. (2009). Made-to-order spiking neuron model equipped with a multi-timescale adaptive threshold. *Frontiers in Comput. Neurosci., 3*(9). doi:10.3389/neuro.10.009.209.

Kohn, A., & Smith, M. (2005). Stimulus dependence of neuronal correlation in primary visual cortex of the macaque. *J. Neurosci., 25*(14), 3661–3663.

Kuhn, A., Aertsen, A., & Rotter, S. (2003). Higher-order statistics of input ensembles and the response of simple model neurons. *Neural Comput., 15*(1), 67–101.

Kuhn, A., Aertsen, A., & Rotter, S. (2004). Neuronal integration of synaptic input in the fluctuation-driven regime. *J. Neurosci., 24*(10), 2345–2356.

Lamme, V., & Roelfsema, P. (2000). The distinct modes of vision offered by feedforward and recurrent processing. *Trends Neurosci., 23*(11), 571–579.

Lancaster, H. (1957). Some properties of the bivariate normal distribution considered in the form of a contingency table. *Biometrika, 44*(1), 289–292.

Litvak, V., Sompolinsky, H., Segev, I., & Abeles, M. (2003). On the transmission of rate code in long feedforward networks with excitatory-inhibitory balance. *J. Neurosci., 23*(7), 30063015.

Ly, C. & Ermentrout, G. (2009). Synchronization dynamics of two coupled neural oscillators receiving shared and unshared noisy stimuli. *Journal of Computational Neuroscience, 26*(3), 425–443.

Maršálek, P., Koch, C., & Maunsell, J. (1997). On the relationship between synaptic input and spike output jitter in individual neurons. *Proc. Natl. Acad. Sci. USA, 94*(2), 735–740.

Mason, A., Nicoll, A., & Stratford, K. (1991). Synaptic transmission between individual pyramidal neurons of the rat visual cortex in vitro. *J. Neurosci., 11*(1), 72–84.

Maynard, E., Hatsopoulos, N., Ojakangas, C., Acuna, B., Sanes, J., Normann, R., et al. (1999). Neuronal interactions improve cortical population coding of movement direction. *J. Neurosci., 19*(18), 8083–8093.

Métivier, M. (1982). *Semimartingales: A course on stochastic processes*. New York: Walter de Gruyter.

Moreno-Bote, R., & Parga, N. (2006). Auto- and crosscorrelograms for the spike response of leaky integrate-and-fire neurons with slow synapses. *Phys. Rev. Lett., 96*(2), 028101.

Moreno-Bote, R., & Parga, N. (2010). Response of integrate-and-fire neurons to noisy inputs filtered by synapses with arbitrary timescales: Firing rate and correlations. *Neural Comp., 22*(6), 1528–1572.

Nawrot, M., Boucsein, C., Molina, V., Riehle, A., Aertsen, A., & Rotter, S. (2008). Measurement of variability dynamics in cortical spike trains. *J. Neurosci. Methods, 169*(2), 374–390.

Okun, M., & Lampl, I. (2008). Instantaneous correlation of excitation and inhibition during ongoing and sensory-evoked activities. *Nat. Neurosci., 11*(5), 535–537.

Ostojić, S., Brunel, N., & Hakim, V. (2009). How connectivity, background activity, and synaptic properties shape the cross-correlation between spike trains. *J. Neurosci., 29*(33), 10234–10253.

Oswald, A., Doiron, B., Rinzel, J., & Reyes, A. (2009). Spatial profile and differential recruitment of $GABA_B$ modulate oscillatory activity in auditory cortex. *J. Neurosci., 29*(33), 10321.

Paninski, L. (2006). The most likely voltage path and large deviations approximations for integrate-and-fire neurons. *J. Comput. Neurosci., 21*(1), 71–87.

Rangan, A. (2009). Diagrammatic expansion of pulse-coupled network dynamics. *Phys. Rev. Lett., 102*(15), 158101.

Rauch, A., La Camera, G., Luscher, H., Senn, W., & Fusi, S. (2003). Neocortical pyramidal cells respond as integrate-and-fire neurons to in vivo-like input currents. *Journal Neurophys., 90*(3), 1598–1612.

Renart, A., Brunel, N., & Wang, X. (2003). Mean-field theory of irregularly spiking neuronal populations and working memory in recurrent cortical networks. In J. Feng (Ed.), *Computational neuroscience: A comprehensive approach.* Boca Raton, FL: CRC Press.

Renart, A., de la Rocha, J., Bartho, P., Hollender, L., Parga, N., Reyes, A., et al. (2010). The asynchronous state in cortical circuits. *Science, 327*, 587–590.

Reyes, A. (2003). Synchrony-dependent propagation of firing rate in iteratively constructed networks in vitro. *Nat. Neurosci., 6*(6), 593–599.

Ringach, D., & Malone, B. (2007). The operating point of the cortex: Neurons as large deviation detectors. *J. Neurosci., 27*(29), 7673–7683.

Rosenbaum, R., Trousdale, J., & Josić, K. (2010). Pooling and correlated neural activity. *Frontiers in Comput. Neurosci, 4*(9), 9 doi:10.3389/fncom.2010.00009.

Roudi, Y., Nirenberg, S., & Latham, P. (2009). Pairwise maximum entropy models for studying large biological systems: When they can work and when they can't. *PLoS Comput. Biol., 5*(5), e1000380.

Salinas, E., & Sejnowski, T. (2000). Impact of correlated synaptic input on output firing rate and variability in simple neuronal models. *J. Neurosci., 20*(16), 6193–6209.

Salinas, E., & Sejnowski, T. (2002). Integrate-and-fire neurons driven by correlated stochastic input. *Neural Comput., 14*(9), 2111–2155.

Schneider, A., Lewis, T., & Rinzel, J. (2006). Effects of correlated input and electrical coupling on synchrony in fast-spiking cell networks. *Neurocomputing, 69*(10–12), 1125–1129.

Schneidman, E., Berry, M., Segev, R., & Bialek, W. (2006). Weak pairwise correlations imply strongly correlated network states in a neural population. *Nature, 440*(7087), 1007–1012.

Shadlen, M., & Newsome, W. (1998). The variable discharge of cortical neurons: Implications for connectivity, computation, and information coding. *J. Neurosci., 18*(10), 3870–3896.

Shea-Brown, E., Josić, K., de La Rocha, J., & Doiron, B. (2008). Correlation and synchrony transfer in integrate-and-fire neurons: Basic properties and consequences for coding. *Phys. Rev. Lett., 100*(10), 108102.

Shlens, J., Field, G., Gauthier, J., Greschner, M., Sher, A., Litke, A., et al. (2009). The structure of large-scale synchronized firing in primate retina. *J. Neurosci., 29*(15), 5022–5031.

Shlens, J., Field, G., Gauthier, J., Grivich, M., Petrusca, D., Sher, A., et al. (2006). The structure of multi-neuron firing patterns in primate retina. *J. Neurosci., 26*(32), 8254–8266.

Sompolinsky, H., Yoon, H., Kang, K., & Shamir, M. (2001). Population coding in neuronal systems with correlated noise. *Phys. Rev. E, 64*(5 Pt. 1), 051904.

Stratonovich, R. (1963). *Topics in the theory of random noise*. London: Gordon & Breach.

Stroeve, S., & Gielen, S. (2001). Correlation between uncoupled conductance-based integrate-and-fire neurons due to common and synchronous presynaptic firing. *Neural Comput., 13*(9), 2005–2029.

Tang, A., Jackson, D., Hobbs, J., Chen, W., Smith, J., Patel, H., et al. (2008). A maximum entropy model applied to spatial and temporal correlations from cortical networks in vitro. *J. Neurosci., 28*(2), 505–518.

Tchumatchenko, T., Malyshev, A., Geisel, T., Volgushev, M., & Wolf, F. (2008). Correlations and synchrony in threshold neuron models. *arXiv*, q-bio.NC.

Temereanca, S., Brown, E., & Simons, D. (2008). Rapid changes in thalamic firing synchrony during repetitive whisker stimulation. *J. Neurosci., 28*(44), 11153–11164.

Thomson, A. (2000). Facilitation, augmentation and potentiation at central synapses. *Trends Neurosci., 23*(7), 305–312.

Tuckwell, H. (1988). *Introduction to theoretical neurobiology*. Cambridge: Cambridge University Press.

Vaadia, E., Haalman, I., Abeles, M., Bergman, H., Prut, Y., Slovin, H., et al. (1995). Dynamics of neuronal interactions in monkey cortex in relation to behavioural events. *Nature, 373*(6514), 515–518.

Vilela, R., & Lindner, B. (2009). Comparative study of different integrate-and-fire neurons: Spontaneous activity, dynamical response, and stimulus-induced correlation. *Phys. Rev. E, 80*(3), 031909.

Zohary, E., Shadlen, M., & Newsome, W. (1994). Correlated neuronal discharge rate and its implications for psychophysical performance. *Nature, 370*(6485), 140–143.

Received June 24, 2010; accepted October 18, 2010.